

Shedding X-ray light on the role of magnesium in the activity of *M. tuberculosis* salicylate synthase (MbtI) for drug design

Matteo Mori, Giovanni Stelitano, Arianna Gelain, Elena Pini, Laurent R. Chiarelli, José Camilla Sammartino, Giulio Poli, Tiziano Tuccinardi, Giangiacomo Beretta, Alessio Porta, Marco Bellinzoni, Stefania Villa, and Fiorella Meneghetti

J. Med. Chem., **Just Accepted Manuscript** • DOI: 10.1021/acs.jmedchem.0c00373 • Publication Date (Web): 12 Jun 2020

Downloaded from pubs.acs.org on June 16, 2020

Just Accepted

“Just Accepted” manuscripts have been peer-reviewed and accepted for publication. They are posted online prior to technical editing, formatting for publication and author proofing. The American Chemical Society provides “Just Accepted” as a service to the research community to expedite the dissemination of scientific material as soon as possible after acceptance. “Just Accepted” manuscripts appear in full in PDF format accompanied by an HTML abstract. “Just Accepted” manuscripts have been fully peer reviewed, but should not be considered the official version of record. They are citable by the Digital Object Identifier (DOI®). “Just Accepted” is an optional service offered to authors. Therefore, the “Just Accepted” Web site may not include all articles that will be published in the journal. After a manuscript is technically edited and formatted, it will be removed from the “Just Accepted” Web site and published as an ASAP article. Note that technical editing may introduce minor changes to the manuscript text and/or graphics which could affect content, and all legal disclaimers and ethical guidelines that apply to the journal pertain. ACS cannot be held responsible for errors or consequences arising from the use of information contained in these “Just Accepted” manuscripts.

1
2
3
4
5
6
7
8
9
10
11
12
13
14
15
16
17
18
19
20
21
22
23
24
25
26
27
28
29
30
31

Shedding X-Ray Light on the Role of Magnesium in the Activity of *M. tuberculosis* Salicylate Synthase (MbtI) for Drug Design

32
33
34
35
36
37
38
39
40
41
42
43
44
45
46
47
48
49
50
51
52
53
54
55
56
57
58
59
60

Matteo Mori^{a,§}, Giovanni Stelitano^{b,§}, Arianna Gelain^a, Elena Pin^a, Laurent R. Chiarelli^b,

José C. Sammartino^b, Giulio Pol[†], Tiziano Tuccinardi^{c,d}, Giangiaco Beretta^e, Alessio

Porta^f, Marco Bellinzon^{g,}, Stefania Villa^{a,*}, Fiorella Meneghetti^a*

^a Dipartimento di Scienze Farmaceutiche, Università degli Studi di Milano, via L.

Mangiagalli 25, 20133 Milano; Italy.

^b Dipartimento di Biologia e Biotechnologie "Lazzaro Spallanzani", Università degli Studi

di Pavia, via A. Ferrata 9, 27100 Pavia; Italy.

^c Dipartimento di Farmacia, Università di Pisa, via Bonanno Pisano 6, 56126 Pisa; Italy.

1
2
3
4 ^d Sbarro Institute for Cancer Research and Molecular Medicine, Center for
5
6
7 Biotechnology, College of Science and Technology, Temple University, Philadelphia,
8
9
10 PA 19122; USA.

11
12
13
14
15 ^e Dipartimento di Scienze e Politiche Ambientali, Università degli Studi di Milano, via G.
16
17
18 Celoria 2, 20133 Milano; Italy.

19
20
21
22 ^f Dipartimento di Chimica, Università degli Studi di Pavia, via T. Taramelli 12, 27100
23
24
25
26 Pavia; Italy.

27
28
29
30 ^g Unité de Microbiologie Structurale, Institut Pasteur, CNRS, Université de Paris, F-
31
32
33
34 75015 Paris; France.

35
36
37
38 **KEYWORDS.** Tuberculosis, magnesium, divalent cations, antitubercular agents, MST
39
40
41 enzymes, catalytic mechanism, siderophores, X-ray crystal structures, mycobactins,
42
43
44
45 MbtI conformations.

46
47
48
49
50 **ABSTRACT.** The Mg²⁺-dependent salicylate synthase (MbtI) from *Mycobacterium*
51
52
53 *tuberculosis* is a key enzyme involved in the biosynthesis of siderophores. Because iron
54
55
56
57
58
59
60

1
2
3 is essential for the survival and pathogenicity of the microorganism, this protein
4
5
6
7 constitutes an attractive target for antitubercular therapy, also considering the absence
8
9
10 of homologous enzymes in mammals. An extension of the SAR of our furan-based
11
12
13 candidates allowed us to disclose the most potent competitive inhibitor known to date
14
15
16
17 (10, $K_i = 4 \mu\text{M}$), which also proved effective on mycobacterial cultures. By structural
18
19
20 studies, we characterized its unexpected Mg^{2+} -independent binding mode. We also
21
22
23 investigated the role of the Mg^{2+} cofactor in catalysis, analyzing the first crystal structure
24
25
26
27 of the MbtI- Mg^{2+} -salicylate ternary complex. Overall, these results pave the way for the
28
29
30 development of novel antituberculars through the rational design of improved MbtI
31
32
33 inhibitors.
34
35
36
37
38
39

40 INTRODUCTION

41
42
43 Nowadays, tuberculosis (TB) ranks among the top ten causes of death worldwide;
44
45
46 therefore, the development of new scaffolds is imperative to sustain the drug pipeline,
47
48
49 considering the issues of the available antitubercular therapies and the increasing
50
51
52 emergence of resistant infections.¹ The salicylate synthase (MbtI) from *Mycobacterium*
53
54
55
56
57
58
59
60

1
2
3
4 *tuberculosis* (Mtb, the etiological agent of TB) is the first enzyme involved in the
5
6
7 biosynthesis of mycobactins. These small-molecule siderophores are capable of
8
9
10 chelating iron, a key cofactor involved in several mycobacterium-specific biological
11
12
13
14 processes. MbtI has been structurally and biochemically characterized,² it is essential
15
16
17 for the survival of Mtb under iron-deficient conditions,³ and, as such, it has been
18
19
20 identified as a promising therapeutic target.⁴
21
22
23
24

25
26 MbtI belongs to the group of the structurally homologous Mg²⁺-dependent
27
28
29 menaquinone, siderophore and tryptophan (MST) enzymes, which transform chorismate
30
31
32 by rearrangement, to generate precursor molecules for the respective biosynthetic
33
34
35 pathways.^{5,6} In this context, MbtI catalyzes the two-step conversion of chorismate to
36
37
38 salicylate, *via* isochorismate as intermediate, performing an isomerase activity followed
39
40
41
42
43 by a lyase activity (Figure 1).⁴
44
45
46

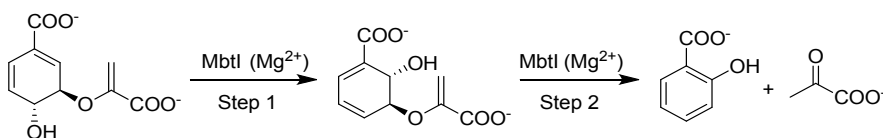
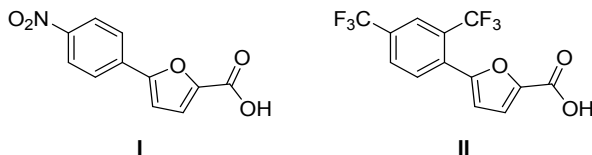


Figure 1. Reactions catalyzed by MbtI.

1
2
3
4 Several strategies have been adopted for the discovery of MbtI inhibitors. In particular,
5
6
7 dicarboxylate substrate analogs (chorismate and isochorismate), transition state
8
9
10 analogs and compounds originated from HTS have been identified.⁷⁻¹⁰ However, these
11
12
13
14 compounds, albeit active against the isolated enzyme, show modest effects on the
15
16
17 whole mycobacterial cell.⁷⁻¹⁰ Notably, Methyl-AMT ($IC_{50} = 11.6 \mu\text{M}$), the best MbtI
18
19
20 inhibitor discovered to date not belonging to our furan-based class, exhibited a poor
21
22
23
24 minimum inhibitory concentration ($MIC^{50} \geq 1 \text{ mM}$), which remained weak ($MIC^{50} = 792$
25
26
27 μM) for its more lipophilic dimethyl ester analog as well.⁴
28
29
30

31
32 Therefore, in order to find improved MbtI inhibitors, we followed an *in silico* screening
33
34
35 approach, which led to the identification of a new hit.¹¹ While exploring the chemical
36
37
38 space around this compound in the frame of a thorough structure-activity relationship
39
40
41 (SAR) study, we discovered two effective derivatives, I and II (Figure 2), which are, to
42
43
44 our knowledge, the most potent MbtI inhibitors reported to date ($IC_{50} = 7.6 \pm 1.6 \mu\text{M}$ and
45
46
47 $13.1 \pm 2.0 \mu\text{M}$, respectively). This strong inhibition of MbtI is correlated to a lethal effect
48
49
50 on Mtb cultures ($MIC^{99} = 156 \mu\text{M}$ and $250 \mu\text{M}$, respectively).^{11,12} Furthermore, the
51
52
53
54
55
56 Universal CAS assay confirmed the connection between the antimycobacterial effect of
57
58
59
60

1
2
3 these compounds and the disruption of mycobactin biosynthesis, thus highlighting the
4
5
6
7 importance of this pathway as a target for the development of therapeutic interventions.
8
9
10 Moreover, we demonstrated the possibility of removing one of the carboxylic groups of
11
12
13
14 Methyl-AMT, without causing a loss in the inhibitory potency and allowing, at the same
15
16
17 time, a better permeability through the cell wall of Mtb.^{11,12}
18
19
20
21



29 **Figure 2.** Chemical structures of compounds I and II.
30
31
32
33

34 Despite the promising results obtained in the inhibition of this target,⁴ its mechanism
35
36 of action is still poorly understood and not supported by conclusive experimental data.
37
38 In particular, a robust definition of the role of Mg²⁺ in the interaction between MbtI and
39
40 inhibitors is still lacking. It has been reported that the affinity of the MST enzymes EntC,
41
42 PchA and Irp9 for ligands is much higher than that for the metal ion, so the driving
43
44 element of the catalytic reaction is the binding of the substrate, followed by interaction
45
46
47
48 with the cofactor.⁶ After the conversion of chorismate to isochorismate, a sudden
49
50
51
52
53
54
55
56
57
58
59
60

1
2
3
4 change in the affinity for the metal occurs: Mg^{2+} is retained by MST enzymes with an
5
6
7 extremely high affinity, promoting the subsequent reaction which quickly leads to the
8
9
10 formation of salicylate.⁶
11
12

13
14 Stimulated by these findings, we started to consider if I and II may participate in the
15
16
17 inhibition mechanism by occupying the active site of the free MbtI before the
18
19
20 intervention of the Mg^{2+} ion, thus blocking the isomerase activity. In this work, we
21
22
23
24 provide experimental data to explain the role of Mg^{2+} on the activity and inhibition of
25
26
27 MbtI. Firstly, we expanded our library of furan-based compounds, designing and
28
29
30 synthesizing new *meta*-derivatives. Among them, the most potent inhibitor identified so
31
32
33
34 far (the *m*-cyano compound **10**, Table 1) was selected as the most suitable candidate to
35
36
37
38 deepen our investigations. The determination of its activity, performed at increasing
39
40
41 concentrations of Mg^{2+} , showed that the metal did not influence the binding of the
42
43
44
45 compound to the target. Then, we updated our computational model, taking into account
46
47
48 the Mg^{2+} -independent binding mode, which allowed us to identify a previously
49
50
51
52 unconsidered key role of some residues. This hypothetical pose was supported by the
53
54
55
56 obtainment of the crystallographic complex of MbtI with **10**, which is here described. As
57
58
59
60

1
2
3 a proof of principle, we also solved a crystal structure of the enzyme in complex with
4
5
6
7 Mg^{2+} , obtained at saturating concentrations of the metal. Moreover, the Mbtl- Mg^{2+}
8
9
10 crystal structure evidenced the presence of salicylate, the product of the enzymatic
11
12
13
14 reaction. Notably, the presence and the interaction pattern of salicylate at the active site
15
16
17 confirmed the hypothesized catalytic mechanism of Mbtl, previously inferred by
18
19
20
21 similarity to other MST enzymes.
22
23
24
25

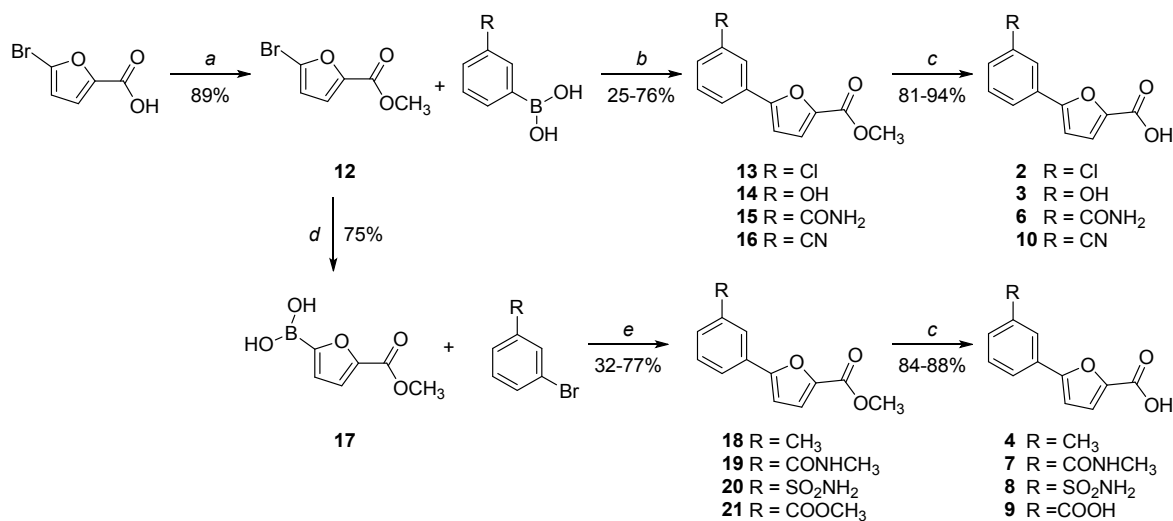
26 RESULTS AND DISCUSSION

27 28 29 *Synthesis and SAR of compounds 1-10*

30
31
32
33 Inspired by the encouraging activity of our leads I and II,^{11,12} we decided to further
34
35
36 explore the phenyl-furan scaffold. In particular, with the aim of obtaining additional SAR
37
38
39 data, we focused on exploring the *meta* position of the phenyl ring using substituents
40
41
42
43 endowed with different stereoelectronic properties, many of which already employed in
44
45
46 our previous studies in which the *ortho* and *para* positions of the phenyl ring were
47
48
49 mainly substituted. Compound 1, bearing only one CF_3 at position 3, was purchased
50
51
52
53 from a commercial source, while 2-10 were synthesized.
54
55
56
57
58
59
60

Compounds **2-4,6-10** were synthesized by a Suzuki-Miyaura reaction,¹¹ either between methyl 5-bromofuran-2-carboxylate and the suitable boronic acid, or between (5-(methoxycarbonyl)furan-2-yl)boronic acid and the appropriate bromo-derivative. The so-obtained esters were hydrolyzed in basic-conditions to yield the free carboxylic acids (Scheme 1). Finally, compound **5** was synthesized from 5-(3-nitrophenyl)furan-2-carboxylate (**23**) through the reduction of its nitro group with tin(II) chloride,¹³ followed by the hydrolysis of the ester function (see Scheme S1 in Supporting Information, SI).

Scheme 1. Synthesis of compounds **2-4, 6-10**.



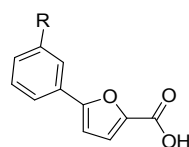
Reagents and conditions: *a*) conc. H₂SO₄, MeOH, reflux, 24 h; *b*) Pd(PPh₃)₂Cl₂, 2M Na₂CO₃, 1,4-dioxane, 90 °C, overnight, N₂; *c*) NaOH, EtOH/THF 1:1, reflux, 5 h or LiOH•H₂O, THF/H₂O 1:1, 20 °C, 2 h. *d*) 1. bis[2-(*N,N*-dimethylamino)ethyl] ether, 2M *i*

1
2
3
4 PrMgCl, THF, 20 min. 10-15 °C – 30 min. r.t., N₂; 2. B(OCH₃)₃, 0 °C, 10 min., N₂; e)
5 Pd(PPh₃)₂Cl₂, 2M Na₂CO₃, 1,4-dioxane, 60 °C, 90 min., MW, N₂.
6
7

8 The activity of compounds 1-10 was tested against recombinant MbtI (Table 1),
9 prepared and assayed as previously reported.¹² Compound 1 showed a promising
10 activity, while the replacement with a halogen (2) or with electron-donating functions like
11 the hydroxyl (3), methyl (4) or amino (5) groups abolished or significantly weakened the
12 activity. The insertion of a strong electron-withdrawing group capable of forming a
13 localized negative charge, like the NO₂ function, previously published (inhibitory activity:
14 50%, at a concentration of 100 μM),¹¹ did not lead to an improvement of the activity.
15
16 Conversely, the amide group of 6 allowed for a significant enhancement of the
17 inhibition, as shown by the IC₅₀ value of 31 μM. While the methylation of the amide in
18 compound 7 led to a strong decrement of the activity, the substitution of the amide with
19 classical bioisosteres (sulfonamide, 8; carboxylic acid, 9) allowed for a retention of the
20 inhibitory effect. Interestingly, the substitution with a nitrile in 10 afforded the best
21 compound of the series, characterized by an IC₅₀ value of about 6 μM; this inhibitor
22
23
24
25
26
27
28
29
30
31
32
33
34
35
36
37
38
39
40
41
42
43
44
45
46
47
48
49
50
51
52
53
54
55
56
57
58
59
60

1
2
3 proved to be slightly better than the previous candidates I and II, thus becoming our
4
5
6
7 improved lead compound.
8
9
10
11
12
13
14
15
16
17
18
19
20
21
22
23
24
25
26
27
28
29
30
31
32
33
34
35
36
37
38
39
40
41
42
43
44
45
46
47
48
49
50
51
52
53
54
55
56
57
58
59
60

Table 1. *m*-Substituted derivatives 1-10. Inhibitory effect is expressed as percentage of residual enzymatic activity (at 100 μ M ligand concentration) for all compounds and Half-Maximal Inhibitory Concentrations (IC_{50} , μ M) only for the most active candidates (residual activity \leq 25%).



Code	R	% Residual activity	IC_{50} (μ M)
1	3-CF ₃	42.0 \pm 6.3	-
2	3-Cl	101.6 \pm 17.8	-
3	3-OH	70.4 \pm 21.8	-
4	3-CH ₃	103.9 \pm 4.8	-
5	3-NH ₂	65.8 \pm 9.6	-
6	3-CONH ₂	20.9 \pm 4.3	31.4 \pm 10.3
7	3-CONHCH ₃	84.0 \pm 9.1	-
8	3-SO ₂ NH ₂	28.6 \pm 6.8	-
9	3-COOH	27.2 \pm 4.5	-
10	3-CN	3.1 \pm 1.0	6.3 \pm 0.9

Biological assays

Compound **10** underwent an in-depth biological evaluation (Figure 3), aimed at characterizing its activity on MbtI and confirming the correlation with a lethal effect on the whole mycobacterial cell. A kinetic analysis confirmed **10** as a competitive inhibitor of MbtI, with a K_i value of $4.2 \pm 0.8 \mu\text{M}$ (Figure 3A). Additional tests were performed to ensure that it was not a PAIN:¹⁴ the addition of BSA and Triton X-100 did not influence the IC_{50} ($6.1 \pm 0.9 \mu\text{M}$ and $5.8 \pm 1.2 \mu\text{M}$, respectively), suggesting that it does not form aggregates with the target. Similarly, the addition of DTT did not impact on the activity of **10** (IC_{50} $7.2 \pm 1.1 \mu\text{M}$), showing that the ligand does not interact with the cysteine residues of the protein (Figure 3B). The antimycobacterial activity of **10** was tested on *M. tuberculosis* H37Rv, providing an MIC^{99} value ($250 \mu\text{M}$) similar to those of the previous inhibitors I and II.¹¹ Moreover, to ascertain that the effects of the compound were due to mycobactin inhibition, **10** was assayed against the non-pathogenic *M. bovis* BCG strain, whose siderophores closely resemble Mtb mycobactins,¹⁵ in iron-limiting conditions, using the chelated Sauton's medium. The compound showed an MIC^{99} value of $250 \mu\text{M}$, and the Universal CAS liquid assay and quantification of the

1
2
3 mycobactins¹⁶ in treated cultures demonstrated that siderophore concentration
4
5
6 decreased at higher concentrations of the compound (Figure 3C and 3D). This
7
8
9 observation confirmed that the inhibitory effect towards mycobacterial growth was due
10
11
12 to mycobactin biosynthesis inhibition. Finally, **10** was screened, following the previously
13
14
15 published procedure,¹² against human MRC-5 fibroblasts to evaluate its cytotoxicity,
16
17
18 revealing an IC₅₀ > 100 μM, thus indicating a low level of toxicity.
19
20
21
22
23
24
25
26
27
28
29
30
31
32
33
34
35
36
37
38
39
40
41
42
43
44
45
46
47
48
49
50
51
52
53
54
55
56
57
58
59
60

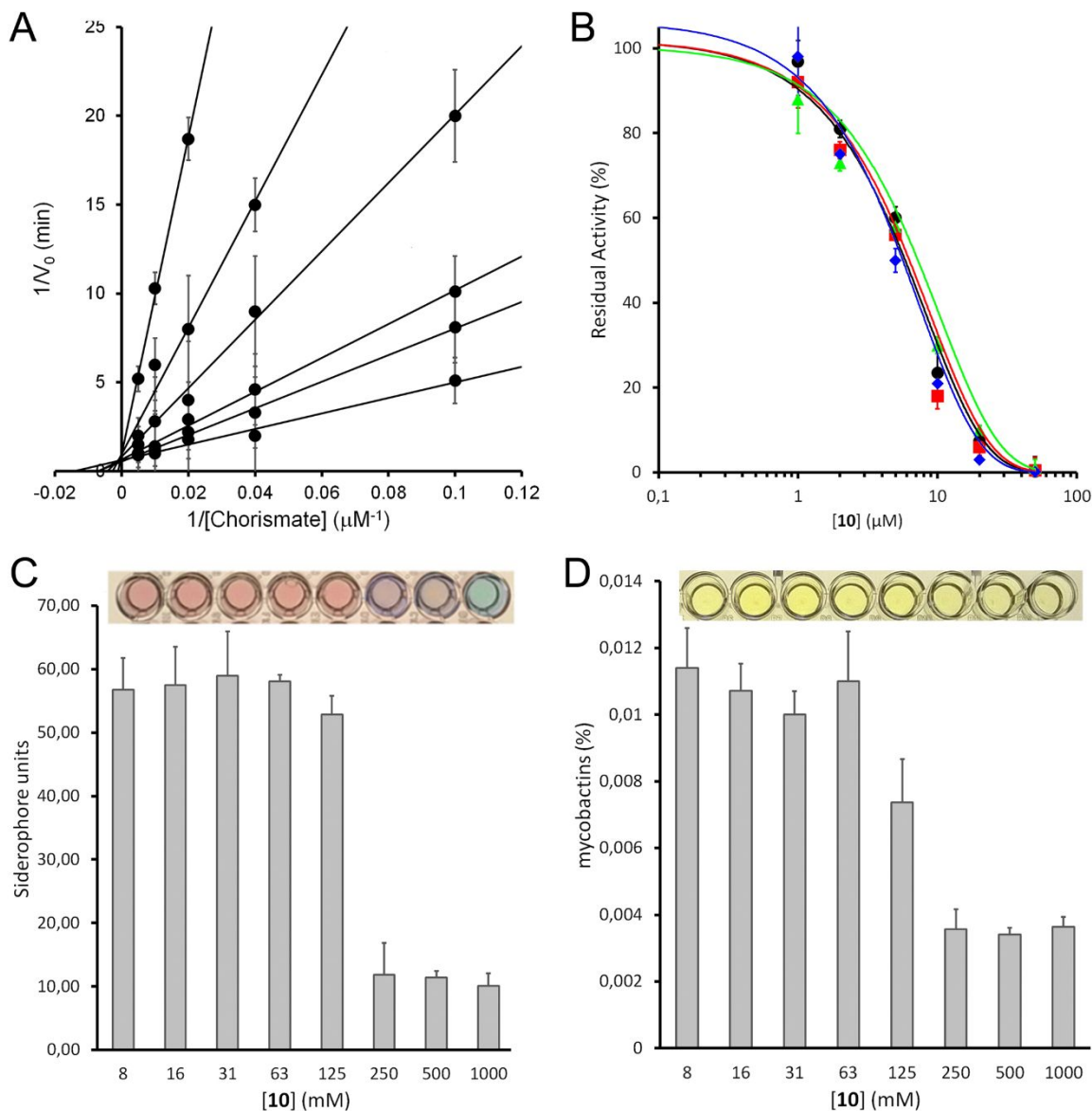


Figure 3. Global reciprocal plot of data from MbtI steady-state kinetics analysis towards chorismic acid, at different concentrations of **10** (A). IC_{50} plot of **10** in the presence of BSA (red), Triton X-100 (green) and DTT (blue) (B). Universal CAS assay performed on *M. bovis* BCG, grown at different concentrations of **10** (C). Determination of

1
2
3 mycobactins in the abovementioned cells. Bars represent mean and standard
4
5
6
7 deviations of three independent experiments (D).
8
9

10 11 *Investigations around the Mg²⁺ ion*

12
13

14 Meneely *et al.*⁶ demonstrated that, in iron-limiting conditions, the affinity of the MST
15
16
17 enzymes EntC, PchA and Irp9 for Mg²⁺ is rather low; hence, the ligand is the first driving
18
19
20
21
22 element of the catalytic reaction. Subsequently, the binding of the Mg²⁺ caps the active
23
24
25
26
27
28 site, thus promoting the initiation of the biosynthetic process. After the conversion of
29
30
31 chorismate to isochorismate, a sudden change in the affinity for the metal occurs: the
32
33
34
35
36
37
38 enzyme tightly binds Mg²⁺, preventing the release of the intermediate and allowing the
39
40
41
42
43
44
45
46
47
48
49
50
51
52
53
54
55
56
57
58
59
60 reaction to quickly evolve towards the formation of salicylate.⁶

39 According to this theory, a ligand endowed with inhibitory properties should therefore
40
41
42
43
44
45
46
47
48
49
50
51
52
53
54
55
56
57
58
59
60 be able to bind to the active site of an MST enzyme, without having to interact with or,
much less, be oriented by the Mg²⁺ ion. On these bases, we undertook an investigation
to verify if such a deduction could be applied to MbtI and to our compounds.
Considering that the presence of Mg²⁺ has been one of the assumptions of most

1
2
3 computational studies regarding MbtI, including ours, we realized that unravelling the
4
5
6
7 binding mechanism of our inhibitors would have a particular significance. In order to
8
9
10 ascertain the likelihood of a Mg^{2+} -independent binding mode for our compounds,
11
12
13 docking experiments, combined with molecular dynamics (MD) simulations, were
14
15
16
17 carried out. The predicted dispositions of **10** into the catalytic site of MbtI was calculated
18
19
20
21 by docking in the absence of the Mg^{2+} ion and then refined through 100 ns of MD
22
23
24 simulation with explicit water molecules (see Experimental Section for details). The
25
26
27
28 results of these studies are shown in Figure 4, which represents the minimized average
29
30
31 structures of **10** within the MbtI binding site. The carboxylic group of the ligand shows
32
33
34 interactions with the hydroxyl group of Tyr385 and the backbone nitrogen of Arg405.
35
36
37
38 The furan oxygen forms a H-bond with Lys438, whereas the benzonitrile fragment
39
40
41
42 shows lipophilic interactions with Ile207, Leu268, Thr361 and an H-bond with Lys205.
43
44
45
46
47
48
49
50
51
52
53
54
55
56
57
58
59
60

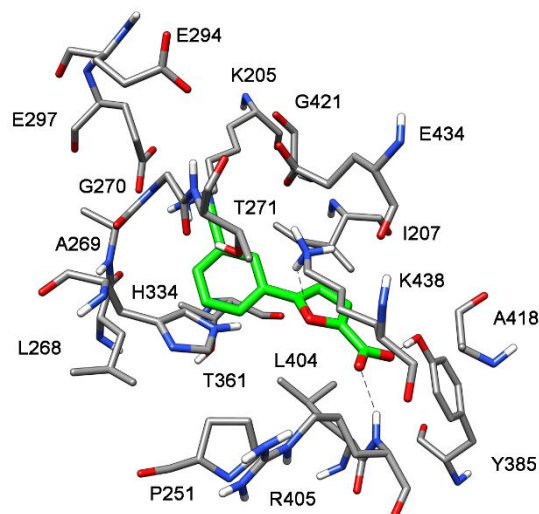


Figure 4. Minimized average structure of **10** within MbtI binding site (PDB ID 3VEH) in absence of the Mg^{2+} ion.

Hence, our modeling approach showed that a Mg^{2+} -independent binding mode was indeed possible, although the exact pose of the ligand could hardly be predicted by a docking/MD simulation study. Therefore, further experimental studies were carried out to characterize the binding mode of our inhibitor.

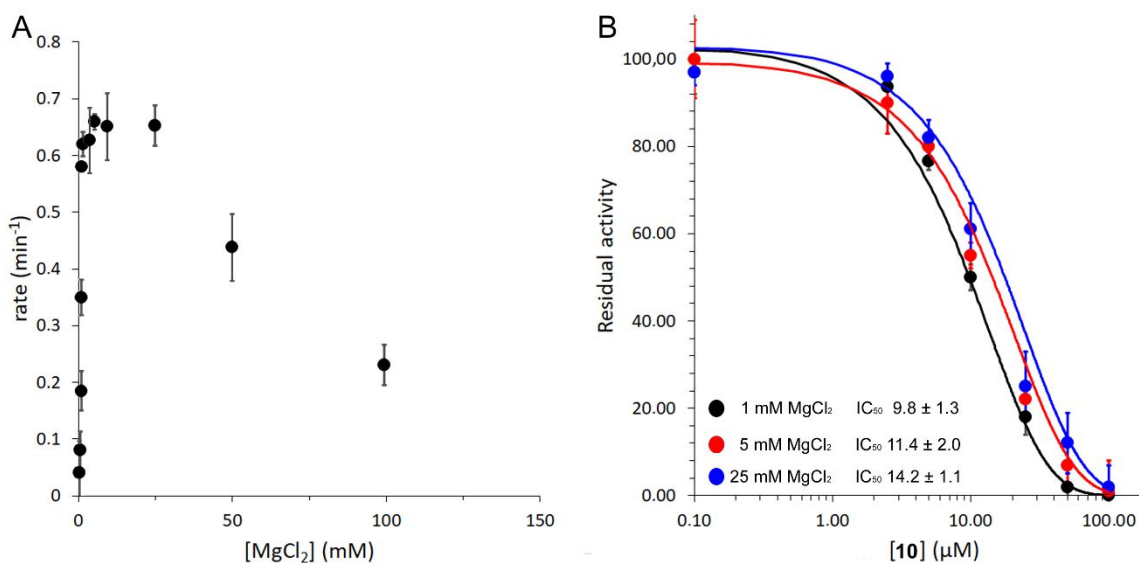
Biochemical investigations on 10

Firstly, we acquired further biochemical data on **10**, testing its activity at different concentrations of Mg^{2+} , with the aim of defining the role of the cofactor in the interaction

1
2
3 between MbtI and the inhibitor. With this strategy, we envisaged that we would observe
4
5
6
7 differences in the inhibitory effect of our ligand in the presence of varying amounts of
8
9
10 Mg^{2+} , if the ion were necessary for its binding and correct orientation in the active site.
11
12
13
14 As expected, MbtI was found to be completely inactive in the absence of its cofactor,
15
16
17 reaching the maximal activity only at 2 mM $MgCl_2$. This result confirmed that the ion is
18
19
20
21 essential for enzymatic activity, although the affinity seems rather moderate. Despite
22
23
24 Ferrer *et al.*^{17,18} reported on the ability of MbtI to act as chorismate mutase in the
25
26
27 absence of the metal, leading to the synthesis of prephenate, our data corroborate the
28
29
30
31 hypothesis formulated by Ziebart and Toney¹⁹ that such activity is likely due to a faulty
32
33
34 purification of the enzyme. Moreover, the use of increasing concentrations of Mg^{2+} (> 50
35
36
37 mM) showed inhibitory effects, as the enzyme activity significantly decreased (Figure 5).
38
39
40
41 Conversely, the enzyme no significant decrease in specific activity when assayed at
42
43
44 concentration of KCl up to 500 mM, confirming that inhibition is specific to Mg^{2+} , and not
45
46
47
48 due to increased ionic strength.
49
50

51
52 The determination of the activity of **10**, performed at different concentrations of Mg^{2+} ,
53
54
55 showed that the metal did not strongly influence the binding of the compound to the
56
57
58
59
60

1
2
3 target. However, in the presence of very high Mg^{2+} concentrations, the performance of
4
5
6
7 **10** was slightly reduced. This observation further supported the hypothesis that at
8
9
10 moderate concentrations of Mg^{2+} , the ligand preferentially binds (and inhibits) MbtI,
11
12
13 while the metal has a low affinity for the enzyme. At high Mg^{2+} concentrations, our data
14
15
16 suggest that the ion nevertheless binds to the active site, occluding the catalytic region
17
18
19 and blocking the access of the inhibitor. These data might also indicate that our
20
21
22 compound could prevent the binding of Mg^{2+} in a competitive fashion, becoming slightly
23
24
25
26
27
28 less effective when the concentration of the metal reaches the higher millimolar range
29
30
31 (Figure 5).



1
2
3
4 **Figure 5.** MbtI enzyme activity as a function of $[Mg^{2+}]$ (A). Profiles of the IC_{50} of **10**,
5
6
7 obtained at different concentrations of Mg^{2+} (B).
8
9

12 *Synthesis and activity of a probe (11)*

15 To date, most MbtI inhibitors reported in the literature, including our candidates, share
16
17
18 a common carboxylate motif that is supposedly responsible for functional sequestration
19
20
21 of the metal ion within the active site.²⁰ However, according to our hypothesis, this
22
23
24 interaction may not be necessary neither for the binding of the ligand, nor for the
25
26
27 resulting inhibitory effect. In order to further verify this theory, we designed and
28
29
30 synthesized a probe molecule, introducing a chemical modification on **10**. The Mg^{2+} ion
31
32
33 is characterized by a small ionic radius, high charge density and tendency to bind water
34
35
36 molecules in the inner coordination sphere, rather than bulkier ligands. Being a “hard”
37
38
39 ion, it prefers to bind “hard” oxygen-containing ligands, such as carbonyls, carboxylates,
40
41
42 phosphates, hydroxyls, and water.²¹ Therefore, the carboxylate pharmacophore motif
43
44
45 was converted to an amide function, affording the analog **11** (see Scheme S2 in SI). Its
46
47
48 docking into MbtI in the absence of Mg^{2+} suggested that a very similar binding mode to
49
50
51
52
53
54
55
56
57
58
59
60

1
2
3 that proposed for **10** was likely (Figure S62). The biological tests on compound **11**
4
5
6 confirmed a very good inhibitory activity ($IC_{50} = 17.3 \pm 1.9 \mu M$), thus supporting our
7
8
9
10 hypothesis that the metal chelation should not be considered an essential
11
12
13
14 pharmacophore feature to develop inhibitors of MbtI.
15
16
17

18 19 *Structure of MbtI in complex with 10*

20
21

22 In the context of our attempts to elucidate the structure of complexes between MbtI
23
24 and 5-phenylfuran-2-carboxylic acid-based inhibitors, we obtained cocrystals with the
25
26
27 lead compound **10**: structural data and refinement statistics are summarized in Table 2.
28
29
30
31

32 These experiments were undertaken to definitively characterize the binding mode of
33
34
35 our candidates, thus providing a reliable means to verify the results of the computational
36
37
38
39 simulations, as well as our previous observations. Furthermore, considering both the
40
41
42 limited size of the compounds and the high plasticity of the active site, we were
43
44
45 convinced that structural studies would assume a particular significance in the
46
47
48
49 identification of the key enzyme-inhibitor interactions.¹²
50
51
52
53
54
55
56
57
58
59
60

1
2
3
4 Among the 3D structures of MbtI available in the PDB, two different conformations
5
6
7 have been reported, which have been described as “open” (e.g. PDB ID 2G5F)² and
8
9
10 “closed” (e.g. PDB ID 3LOG)⁷, depending on the relative position of two mobile loops
11
12
13 with respect to the active site. In the closed form, the flexible sequences (residues 268-
14
15
16 293 and 324-336)²⁰ are bent over the binding pocket, while in the open form they are
17
18
19 tilted upward. A comparative analysis of previously published structures allowed us to
20
21
22 identify the intermolecular bonds responsible for this conformational shift. In particular,
23
24
25
26
27 the closed state seems to be determined by the formation of a H-bond between a
28
29
30 suitable moiety of the ligand and the NH of Gly270 and/or the hydroxyl group of Thr271:
31
32
33
34
35 these contacts effectively drag the first mobile loop towards the active site. In turn,
36
37
38 Thr271 establishes a bond with His334, thus pulling the second mobile loop in the same
39
40
41 direction. The link between the flexible regions is further stabilized by additional
42
43
44 interactions, formed by adjacent amino acids. Overall, this movement determines the
45
46
47 capping of the active site. The chemical entity responsible for the interaction with
48
49
50
51
52 Gly270 or Thr271 is a carbonate anion (or an ordered water molecule) in 3LOG, and a
53
54
55
56
57
58
59
60 carboxyl group in PDB IDs 3ST6 and 3VEH (chains A, B, C). Interestingly, in PDB IDs

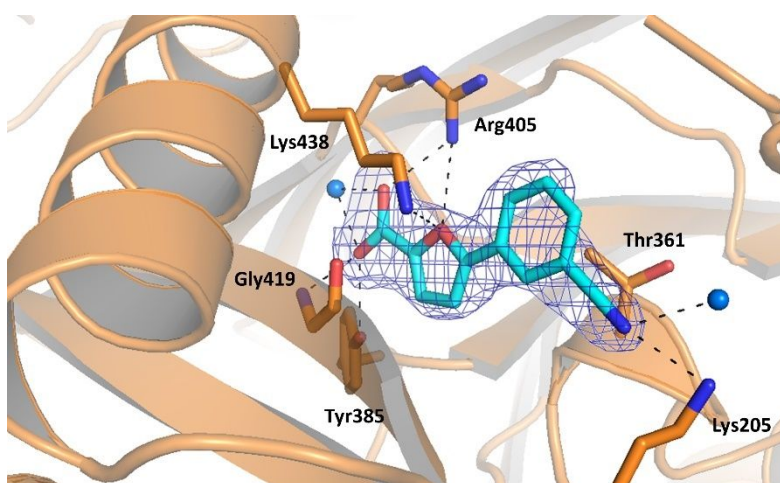
1
2
3 3RV7, 3RV8, 3RV9, the absence of this H-bond induces an open conformation, despite
4
5
6
7 the orientation of the ligands does not differ significantly compared to the one observed
8
9
10 in 3VEH. In chain D of 3VEH, the increased distance between the COOH and Thr271
11
12
13 (3.21 Å vs 2.70-2.89 Å) determines an intermediate conformation. Another intermediate,
14
15
16
17 but overall open state can be observed in 3RV7 chain B, in which a contact between
18
19
20 Thr271 and Ser331 induces a slightly more closed configuration compared to the other
21
22
23 chains. The peculiar binding mode of the bulkier inhibitor of PDB ID 3RV6 determines
24
25
26
27 an unprecedented conformation, in which the opening of the mobile loops is
28
29
30
31 characterized by a particularly wide angle. Notably, these mobile regions are
32
33
34 characterized by high B-factors and partial lack of supporting electron density,
35
36
37 especially when the conformation is open, despite some chains show stabilized
38
39
40 conformations, mostly in the 324-336 loop, due to different crystal packing interactions
41
42
43 involving these regions.
44
45
46
47
48

49 In the complex MbtI-10, the enzyme conformation can be defined as an open state for
50
51
52 the ensemble of the four molecules in the ASU, despite the partially incomplete electron
53
54
55 density of the mobile loops (unresolved regions for chain A: 271-276; chain B: 270-290
56
57
58
59
60

1
2
3 and 328-334; chain C: 275-282; chain D: 274-277). The adoption of this conformation is
4
5
6
7 due to the fact that **10** does not possess a suitable functional group in the correct
8
9
10 orientation to establish a H-bond with Gly270 or Thr271. Consequently, the
11
12
13 arrangement of the flexible loops of MbtI-**10** is similar to that of 2G5F, 3RV7, 3RV8, and
14
15
16
17 3RV9, with root-mean-square deviations in the range 1-4 Å (calculated for residues 325-
18
19
20
21 335).

22
23
24 An electron density compatible with the presence of the ligand is detectable in all four
25
26
27 chains of the ASU, with the furan-2-carboxylic acid region always well-defined, and
28
29
30
31 weaker electron density for the phenyl portion. The analysis of the binding mode of the
32
33
34 compound revealed the presence of H-bonds between its carboxylic group and Tyr385,
35
36
37 Arg405, and an ordered water molecule; the oxygen of the furan interacts with Arg405,
38
39
40
41 while the phenyl ring forms a cation- π interaction with Lys438 and a Van der Waals
42
43
44 contact with Thr361. Finally, the cyano group forms a H-bond with Lys205, a key amino
45
46
47 acid involved in the first step of the catalytic reaction (Figure 6). This residue is likely
48
49
50 responsible for the activation of a water molecule for nucleophilic attack (S_N2) on C2 of
51
52
53 chorismate, which leads to the release of the hydroxyl group at position 4, after its
54
55
56
57
58
59
60

1
2
3
4 protonation mediated by Glu252, thereby affording isochorismate.²² One may speculate
5
6
7 that the absence of an interaction with the pivotal Lys205 in isochorismate-based
8
9
10 derivatives accounts for their slightly weaker inhibitory activity with respect to **10**. The
11
12
13 superposition of MbtI-**10** with 3RV7 (Figure S54) shows that the arrangement of the
14
15
16 amino acid side chains around the ligands is similar, with the aromatic carboxylic group
17
18
19 of the AMT derivative occupying the same position as the acid moiety of **10**. The most
20
21
22 significant difference is represented by the ability of the nitrile group of **10** to form a H-
23
24
25 bond with Lys205, thereby hindering its physiological functions.
26
27
28
29
30
31
32



33
34
35
36
37
38
39
40
41
42
43
44
45
46
47
48
49
50 **Figure 6.** Ribbon diagram of the MbtI-**10** structure (PDB ID 6ZA4): the interactions of the
51
52
53 ligand with the side chains (in sticks) and the water molecules (blue spheres) are
54
55
56
57
58
59
60

1
2
3 represented as dashed lines. The blue mesh represents the electron density around the
4
5
6
7 ligand (contoured at 1σ).
8
9

10
11
12 Despite our experiments were carried out in the presence or in the absence of Mg^{2+} in
13
14
15 the crystallization buffer (2-5 mM of different Mg^{2+} salts), we never observed any bound
16
17
18 Mg^{2+} in the MbtI-**10** cocrystal structure. The orientation of the ligand is substantially in
19
20
21 agreement with the predicted binding mode of **10** in the absence of Mg^{2+} , as shown by
22
23
24
25 the overlay of the two models (Figure S55). The binding poses in the two complexes
26
27
28 exhibit a root-mean-square deviation of 1.6 Å and similar interactions. The main
29
30
31 differences are related to the orientation of the side chain of Arg405, which was not
32
33
34 predicted to interact with the ligand, as well as the side chains of Thr271 and His334,
35
36
37 which are shifted away from the binding site. As previously mentioned, the absence of
38
39
40 interactions between the ligand with the amide group of Gly270 or the hydroxyl group of
41
42
43 Thr271 seems to favor the outward movement of the backbone in the two mobile loops,
44
45
46 thereby leading to an open conformation. Such shift could hardly be predicted by
47
48
49
50
51
52
53 computational simulations, as those were based on a closed form of the enzyme. As for
54
55
56
57
58
59
60

1
2
3
4 Arg405, the analysis of electron density indicates a high flexibility of its side chain,
5
6
7 which is otherwise modeled, where supporting density is present, as different rotamers.
8
9
10

11 *Structure of MbtI with the Mg²⁺ ion*

12
13
14

15 Although the role of the Mg²⁺ cofactor in the catalytic activity of MbtI has been the
16
17
18 subject of a number of publications,⁴ its role remains elusive. Our numerous attempts to
19
20
21 obtain a structure of MbtI in ternary complex with **10** and Mg²⁺ failed, invariably leading
22
23
24 to the cocrystal described above. Notably, the only available structure of MbtI showing a
25
26
27 bound Mg²⁺ ion was obtained by Chi and co-workers (3RV6).²⁰ However, as stated by
28
29
30 the authors, its binding mode under those conditions may not necessarily reproduce the
31
32
33 physiological situation: the ion was found to be hexacoordinated by water molecules,
34
35
36 interacting with the enzyme and the inhibitor only through the surrounding waters,
37
38
39
40
41
42
43 inconsistently with both its supposed role in catalysis¹⁸ and the authors' predicted
44
45
46 binding mode. Therefore, we decided to further pursue the investigation of the binding
47
48
49 and coordination of Mg²⁺ into the active site of MbtI, in order to clarify its role in the
50
51
52 enzymatic mechanism.
53
54
55
56
57
58
59
60

1
2
3
4 Considering the inherent difficulty in obtaining Mbtl-Mg²⁺ cocrystals, as well as the
5
6
7 results of our biochemical assays, we hypothesized that we could compensate for the
8
9
10 rather low affinity of Mbtl for its cofactor by using saturating concentrations of Mg²⁺.
11
12
13 Interestingly, 2.1 Å resolution data were collected from a non-isomorphous crystal
14
15
16
17 grown under these conditions (Table 2).
18
19
20

21 The crystal structure derived from these data presents four molecules in the ASU, with
22
23
24 a well-defined electron density in all regions, including the previously observed mobile
25
26
27 loops that are now stabilized into a closed conformation, superimposable with the one
28
29
30 observed in 3LOG or 3ST6.^{7,20} The analysis of the active site evidenced electron
31
32
33 density fully consistent with the presence of a Mg²⁺ ion, though its coordination sphere
34
35
36 is slightly different in the various chains. In chain A (Figure S56), the Mg²⁺ interacts with
37
38
39 the oxygen of Gly421, with four ordered water molecules, and with a sulfate anion.
40
41
42 Through two of the water molecules, it also contacts Glu431 and Glu434. Chain C does
43
44
45 not show the presence of the ion; in its absence, Glu431 binds a water molecule and
46
47
48 there is no clear electron density for the side chain of Glu434. The coordination pattern
49
50
51 of Mg²⁺ in chains B and D is analogous (Figure 7): the ion could be modeled as directly
52
53
54
55
56
57
58
59
60

1
2
3 interacting with Glu297, Glu434, and two ordered water molecules, which in turn make
4
5
6
7 H-bonds to Glu294 and Glu431. In addition to that, the metal forms a strong interaction
8
9
10 with another molecule, which, by analogy with the crystal structure of Irp9 from *Yersinia*
11
12
13 *enterocolitica* (PDB ID 2FN1), could be identified and modeled as a salicylate.²³
14
15
16
17 Supporting density for the bound catalytic product could be identified in two protein
18
19
20 chains over four, where the pose of the refined ligand was perfectly superimposable to
21
22
23 that of 2FN1 (Figure S57). The salicylate coordinates the Mg²⁺ ion with its carboxylic
24
25
26
27 moiety, which also forms additional H-bonds with the peptide backbone through Gly270
28
29
30 and Gly421, and with the side chain of Thr271. The hydroxyl group and the phenyl ring
31
32
33
34 do not seem to form significant interactions. As previously noted, the bond between the
35
36
37
38 carboxylic function and Gly270-Thr271 is responsible for the adoption of the closed
39
40
41
42 conformation (Figure 8). The comparison of this structure with MbtI-10 and 3RV7
43
44
45 showed a moderate rearrangement of the residues in the active site (Figure S58). Both
46
47
48
49 the side chains of the interacting amino acids and some portions of the main chain
50
51
52 backbone (Gly270) are tightened around the ion and salicylate, narrowing the binding
53
54
55
56 pocket. The orientation of the salicylate is almost orthogonal to the plane formed by the
57
58
59
60

1
2
3 rings of the inhibitors. Therefore, the aromatic carboxylic groups of the ligands and the
4
5
6
7 carboxylate of the natural product do not occupy the same position: instead, the acidic
8
9
10 moiety of the inhibitors is here replaced by a sulfate anion. Conversely, the aliphatic
11
12
13
14 carboxylic function in 3RV7 may be oriented towards the ion by rotation around the
15
16
17 ether bond. The superposition of our Mg^{2+} -bound structure with the closed structures
18
19
20
21 3VEH and 3ST6 showed a much similar arrangement of the residues in the binding
22
23
24 pocket, with the exception of some amino acids involved in the binding of Mg^{2+} , which
25
26
27 are tilted away in the literature structures (Figure S59). Moreover, while the orientation
28
29
30
31 of the compound in 3VEH is comparable to that of 3RV7, the position of the aromatic
32
33
34 analogue of isochorismate in 3ST6 is overturned, with the aromatic portion occupying
35
36
37
38 roughly the same position as the salicylate. This is the only AMT derivative which
39
40
41
42 exhibits such an orientation. As mentioned above, the side chain of Arg405 also shows
43
44
45
46 deviations due to its flexibility.
47
48
49
50
51
52
53
54
55
56
57
58
59
60

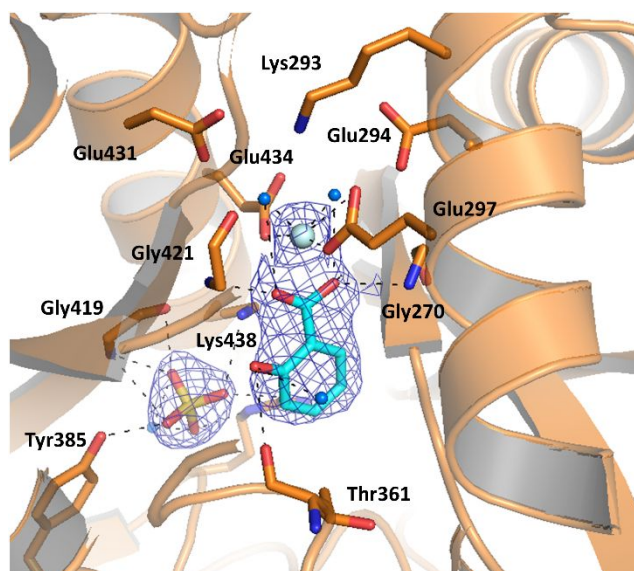


Figure 7. Ribbon diagram of the MbtI-Mg²⁺ structure (PDB ID 6ZA5), focused on the active site of chain D. The interactions of the ligands with the side chains (in sticks), the Mg²⁺ ion (light blue sphere) and the water molecules (blue spheres) are represented as dashed lines. The blue mesh represents the electron density around the ligand (contoured at 1 σ).

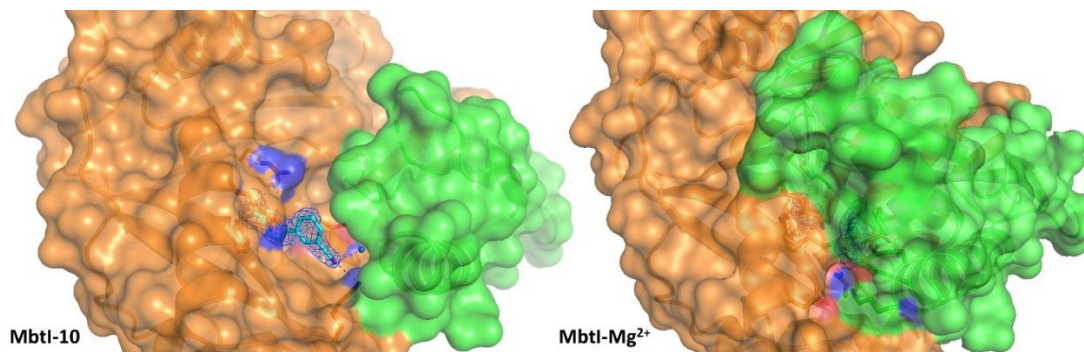


Figure 8. Comparison of surface of Mbtl-10 (left, PDB ID 6ZA4) and Mbtl-Mg²⁺(right, PDB ID 6ZA5), showing the movement of the mobile loops (in green, only partially traced in Mbtl-10 due to the lack of supporting electron density). The active site accessibility determines the conformational state of the enzyme (open, in Mbtl-10, *vs.* closed in Mbtl-Mg²⁺). The blue mesh represents the electron density around active site ligands (contoured at 1 σ); the side chains of the interacting amino acids are in sticks.

The presence of bound salicylate in the structure is remarkable, especially considering that the natural substrate was not added to the crystallization solution. To confirm the presence of a salicylate molecule bound to the protein, Mbtl (25 mg/mL) was heat-denatured to release any bound compound and centrifuged; the resulting supernatant was subjected to UPLH-MS analysis. As shown in Figure S63, a peak

1
2
3
4 corresponding to that of the salicylic acid was detected in the supernatant of the treated
5
6
7 MbtI, and not in controls. This finding suggests that the enzyme is active in the
8
9
10 heterologous expression host (*E. coli*) and that either chorismate or salicylate, both of
11
12
13 which are known to be intermediates in *E. coli* aromatic biosynthetic pathways, is co-
14
15
16 purified with the protein. It is worth to note that the first described crystal structure of
17
18
19 MbtI (2G5F), also reportedly copurified from *E. coli*, showed the presence of pyruvate in
20
21
22 the active site, which thus prompted the authors to classify the enzyme as a salicylate
23
24
25 synthase.² Unsurprisingly, the position that was occupied by the pyruvate is here taken
26
27
28 by a sulfate ion, provided in the crystallization solution as the Mg²⁺ counterion. At
29
30
31 increasing MgCl₂ concentrations the enzyme catalytic turnover is significantly reduced,
32
33
34 strongly supporting the notion that high Mg²⁺ concentrations stabilize the closed
35
36
37 conformation of the active site, preventing the loss of salicylate from the active site.
38
39
40 Besides, the direct salicylate-Mg²⁺ interaction, shown here for the first time for MbtI, is
41
42
43 consistent with biochemical observations on the role of Mg²⁺ by Meneely *et al.*⁶
44
45
46
47
48
49
50
51

52 Furthermore, indirect confirmation of the binding position of Mg²⁺ in the active site of
53
54
55 MbtI was obtained from another structure, solved from crystals grown in the presence of
56
57
58
59
60

1
2
3 chorismate in its commercially available Ba²⁺ salt (Table 2). Despite no evidence of
4
5
6
7 bound chorismate was found from the analysis of the electron density maps, a bound
8
9
10 Ba²⁺ ion was identified (Figure S60). This divalent ion roughly occupies the same
11
12
13 position of Mg²⁺ (Figure S61), further confirming the presence of a metal binding site.
14
15
16
17 Ba²⁺ forms a similar pattern of interactions with the surrounding residues, with slight
18
19
20 modifications due to its different steric hindrance. Moreover, as in the Mg²⁺-bound
21
22
23 structure, the enzyme exhibits the same closed conformation: in this case, the H-bond
24
25
26 with Thr271 is established by an oxygen of a phosphate anion, originating from the
27
28
29 crystallization condition.
30
31
32
33
34
35

36 CONCLUSIONS

37
38
39
40 In this work, we report the discovery of a new pharmacophore model based on the
41
42
43 crystal structure of *Mycobacterium tuberculosis* salicylate synthase (MbtI) complexed
44
45
46 with **10**, the most potent inhibitor discovered to date, also active against isolated
47
48
49 mycobacterial cells. Our experiments proved the connection between its
50
51
52
53 antimycobacterial effect and the disruption of mycobactin biosynthesis, confirming the
54
55
56
57
58
59
60

1
2
3 importance of this pathway as a target for novel anti-TB therapies. The MbtI-10
4
5
6 structure highlighted a new mode of ligand-protein interaction in which the binding of the
7
8
9 ion is not a key feature for the development of improved inhibitors. Moreover, the co-
10
11
12 crystal structure highlighted the importance of fundamental residues for the binding of
13
14
15 the ligand, such as Thr361, Tyr385, Arg405, Lys438, and in particular of Lys205, a key
16
17
18
19 amino acid involved in the first step of the catalytic reaction. These findings constitute
20
21
22 the basis for the development of a novel pharmacophore model for MbtI ligands, which
23
24
25
26 could be profitably employed in virtual screening protocols aimed at the identification of
27
28
29 structurally novel inhibitors and in lead optimization campaigns focused on the
30
31
32 development of more potent analogs of compound 10.
33
34
35
36
37

38 In addition, the X-ray structure of MbtI complexed with Mg^{2+} is consistent with the
39
40
41 proposed mechanism of the enzyme, and, most notably, the role of the Mg^{2+} cofactor.
42
43
44
45 The crystal structure of the ternary complex of MbtI with Mg^{2+} and salicylate shows the
46
47
48 product of the catalytic reaction chelating the metal ion with its carboxylic moiety, and
49
50
51 forming additional H-bonds with Gly270, Gly421, and Thr271. Observing such a
52
53
54
55 conformation in this ternary complex is not surprising when high concentrations of Mg^{2+}
56
57
58
59
60

1
2
3 are present; consistently with previous hypothesis and biochemical data, the bound
4
5
6
7 Mg^{2+} ion stabilizes the enzyme in a close conformation, which in turn prevents the loss
8
9
10 of salicylate from the active site.

11
12
13
14 These findings contribute to fill the gap in the understanding of the kinetic and
15
16
17 chemical mechanisms of this enzyme, supporting the development of high affinity
18
19
20 inhibitors. Given the structural similarity between MbtI and other MST enzymes,
21
22
23 designing new antimicrobials endowed with a multi-target activity is now a foreseeable
24
25
26
27 scenario.

31 32 33 **EXPERIMENTAL SECTION**

34 35 36 *Chemistry*

37
38
39 All starting materials, chemicals and solvents were purchased from commercial
40
41
42 suppliers (Sigma-Aldrich, St. Louis, MI, USA; FluoroChem, Hadfield, UK; Carlo Erba,
43
44
45 Cornaredo, Italy) and used as received. Anhydrous solvents were utilized without further
46
47
48 drying. Aluminum-backed Silica Gel 60 plates (0.2 mm; Merck, Darmstadt, Germany)
49
50
51 were used for analytical thin-layer chromatography (TLC), to follow the course of the
52
53
54
55
56
57
58
59
60

1
2
3 reactions. Microwave-assisted reactions were carried out with a Biotage® Initiator
4
5
6 Classic (Biotage, Uppsala, Sweden). Silica gel 60 (40–63 μm ; Merck) was used for the
7
8
9 purification of intermediates and final compounds, through flash column
10
11
12 chromatography. Melting points were determined in open capillary tubes with a Stuart
13
14
15 SMP30 Melting Point Apparatus (Cole-Parmer Stuart, Stone, UK). All tested compounds
16
17
18 were characterized by means of ^1H NMR, ^{13}C NMR, FT-IR, HRMS. ^1H and ^{13}C NMR
19
20
21 spectra were acquired at ambient temperature with a Varian Oxford 300 MHz
22
23
24 instrument (Varian, Palo Alto, CA, USA), operating at 300 MHz for ^1H and 75 MHz for
25
26
27 ^{13}C . Chemical shifts are expressed in ppm (δ) from tetramethylsilane resonance in the
28
29
30 indicated solvent (TMS: $\delta = 0.0$ ppm), while J -couplings are given in Hertz. The APT
31
32
33 sequence was used when deemed necessary. The 2D-NOESY sequence was
34
35
36 employed to unambiguously assign the hydrogen signals, when appropriate; this
37
38
39 experiment was performed on a Bruker Avance 300 MHz instrument (Bruker, Billerica,
40
41
42 MA, USA). IR spectra were acquired with a Perkin Elmer Spectrum One FT-IR (Perkin
43
44
45 Elmer, Waltham, MA, USA), in a spectral region between 4000 and 450 cm^{-1} and
46
47
48 analyzed by transmittance technique with 32 scans and 4 cm^{-1} resolution. Solid
49
50
51
52
53
54
55
56
57
58
59
60

1
2
3 samples were mixed in a mortar with KBr (1:100) and pressed to small tablets, using a
4
5
6
7 hydraulic press (14 tons). The purity of the final compounds was assessed by means of
8
9
10 LC-High-Resolution Mass Spectrometry (Q Exactive™ Hybrid Quadrupole-Orbitrap™
11
12
13 Mass Spectrometer; Thermo Fischer, Waltham, MA, USA) and was $\geq 95\%$.
14
15

16
17 Compound 1 was purchased from Sigma-Aldrich at the highest purity level available
18
19
20
21 ($\geq 95\%$) and tested as received.
22
23
24
25

26 *General Procedure A. Procedure A1.* The appropriate methyl ester derivative (1
27
28 mmol) was dissolved in a mixture of THF/EtOH 1:1 (15 mL) and a 1 M solution of NaOH
29
30 (2.5 mmol) was added dropwise while stirring. The reaction mixture was heated at reflux
31
32
33 for 5 h. After completion, the solvent was evaporated under reduced pressure; the
34
35
36 aqueous phase was washed with CHCl_3 (1 x 5 mL), acidified with 3 M HCl and then
37
38
39 extracted with EtOAc (3 x 7 mL). The organic layers were washed with brine, dried over
40
41
42 anhydrous Na_2SO_4 and then concentrated *in vacuo*. The resulting solid was washed
43
44
45
46 with cool hexane (3 mL). *Procedure A2.* The appropriate methyl ester derivative (1
47
48
49 mmol) was treated with $\text{LiOH}\cdot\text{H}_2\text{O}$ (3.0 mmol) in a mixture of THF– H_2O 2:1 (15 mL) at
50
51
52
53
54
55
56
57
58
59
60

1
2
3 room temperature for 2 h. After completion, the solution was acidified with 1 M HCl and
4
5
6 then extracted with EtOAc (3 x 7 mL). The organic layers were washed with brine, dried
7
8
9
10 over anhydrous Na₂SO₄ and then concentrated *in vacuo*.^{11,12}
11
12

13
14 *General Procedure B.* The suitable aromatic ester (1 mmol), the appropriate
15
16 phenylboronic acid (1.3 mmol) and bis(triphenylphosphine)palladium(II) dichloride (5%
17
18 mol) were dissolved in dry 1,4-dioxane (10 mL), under N₂ atmosphere. A 2 M Na₂CO₃
19
20
21 solution (2 mmol) was added and the resulting mixture was stirred overnight at 90 °C.
22
23
24 After completion, the solution was cooled to room temperature and then filtered on a
25
26
27 celite pad. The filtrate was diluted with H₂O and extracted with EtOAc (3 x 4 mL). The
28
29
30 organic layer was dried over anhydrous Na₂SO₄, filtered and concentrated *in vacuo*.^{11,12}
31
32
33
34
35
36
37

38
39 *General Procedure C.* Methyl 5-boronofuran-2-carboxylate (**17**, 1.3 mmol), the
40
41 appropriate bromo-derivatives (1.0 mmol) and bis-(triphenylphosphine)palladium(II)
42
43
44 dichloride (5% mol) were dissolved in dry 1,4-dioxane (10 mL), under N₂ atmosphere. A
45
46
47 2 M Na₂CO₃ solution (2 mmol) was then added, and the resulting mixture was stirred in
48
49
50 a microwave synthesizer (Biotage® Initiator Classic) for 1 h at 60 °C. After completion,
51
52
53 the solution was cooled to room temperature and filtered on a celite pad. The filtrate
54
55
56
57
58
59
60

1
2
3 was diluted with H₂O and extracted with EtOAc (3 x 4 mL). The organic layer was dried
4
5
6
7 over anhydrous Na₂SO₄, filtered and concentrated *in vacuo*.^{11,12}
8
9

10 *General procedure D.* The appropriate aromatic carboxylic acid (1 mmol) was
11
12 dissolved in MeOH (4.8 mL) before concentrated H₂SO₄ (0.7 mL) was added dropwise
13
14
15 while stirring. The reaction mixture was refluxed for 24 h. After completion, the solution
16
17
18 was cooled to room temperature and MeOH was removed *in vacuo*; the aqueous phase
19
20
21 was treated with a saturated solution of NaHCO₃ to ensure neutral-basic pH and then
22
23
24 extracted with EtOAc (3 x 4 mL). The combined organic layers were washed with brine,
25
26
27
28 dried over anhydrous Na₂SO₄, filtered and concentrated *in vacuo*.²⁴
29
30
31
32
33

34
35 **5-(3-Chlorophenyl)furan-2-carboxylic acid (2).** Procedure A1. Starting compound:
36
37 methyl 5-(3-chlorophenyl)furan-2-carboxylate (50 mg, 0.21 mmol, **12**). Light brown solid.
38
39 Yield: 42 mg, 0.19 mmol, 89%. Mp: 187 °C (dec.). TLC (DCM–MeOH 8:2): R_f = 0.27. ¹H
40
41
42 NMR (300 MHz, DMSO-*d*₆) δ (ppm): 7.76 (t, *J* = 1.7 Hz, 1H, H₇), 7.67 (d, *J* = 7.7, 1H,
43
44 H₁₁), 7.44 (t, *J* = 7.7 Hz, 1H, H₁₀), 7.33 (d, *J* = 7.7, 1H, H₉), 7.06 (d, *J* = 3.4 Hz, 1H, H₃),
45
46
47 6.88 (s, 1H, H₄). ¹³C NMR (75 MHz, DMSO-*d*₆) δ: 160.72, 160.45, 160.36, 151.98,
48
49
50
51
52
53
54
55
56
57
58
59
60 134.45, 132.97, 131.56, 128.09, 123.92, 122.95, 109.29. FT-IR (KBr) ν cm⁻¹: 3412,

1
2
3
4 2961, 2920, 2851, 1674, 1660, 1602, 1525, 1461, 1420, 1384, 1305, 1278, 776. HRMS
5
6
7 (ESI-QOrbitrap) m/z . calcd. for $C_{11}H_7ClO_3$ $[M-H]^-$, 221.0011. Found 221.0022.
8
9

10 **5-(3-Hydroxyphenyl)furan-2-carboxylic acid (3)**. Procedure A1. Starting compound:
11
12 methyl 5-(3-hydroxyphenyl)furan-2-carboxylate (55 mg, 0.25 mmol, **13**). White solid.
13
14 Yield: 48 mg, 0.24 mmol, 94%. Mp: 170 °C. TLC (DCM–MeOH 7:3): R_f = 0.40. 1H NMR
15
16 (300 MHz, $DMSO-d_6$) δ (ppm): 13.10-13.00 (bs exch. D_2O , 1H, COOH), 9.80-9.60 (bs
17
18 exch. D_2O , 1H, OH), 7.26 (d, J = 3.4 Hz, 1H, H_3), 7.18-7.06 (m, 3H, $H_{7,10,11}$), 7.04 (d, J =
19
20 3.4 Hz, 1H, H_4), 6.77 (dt, J = 7.3, 2.1 Hz, 1H, H_9). ^{13}C NMR (75 MHz, $DMSO-d_6$) δ
21
22 (ppm): 159.72, 158.30, 156.76, 144.46, 130.77, 130.75, 122.18, 116.55, 115.83,
23
24 111.33, 108.19. FT-IR (KBr) ν cm^{-1} : 3401, 2919, 1675, 1649, 1582, 1533, 1470, 1418,
25
26 1309, 1298, 1284, 1200, 1160, 1025, 954, 852, 799, 785. HRMS (ESI-QOrbitrap) m/z .
27
28 calcd for $C_{11}H_9O_4$ $[M+H]^+$, 205.0495. Found 205.0499.
29
30
31
32
33
34
35
36
37
38
39
40
41
42
43
44

45 **5-(*m*-Tolyl)furan-2-carboxylic acid (4)**. Procedure A1. Starting compound: methyl 5-
46
47 (*m*-tolyl)furan-2-carboxylate (48 mg, 0.22 mmol, **18**). Brown solid. Yield: 39 mg, 0.19
48
49 mmol, 86%. Mp: 147 °C. TLC (DCM–MeOH 8:2): R_f = 0.35. 1H NMR (300 MHz, $DMSO-$
50
51 d_6) δ (ppm): 13.07 (bs exch. D_2O , 1H, COOH), 7.62-7.56 (m, 2H, $H_{7,11}$), 7.34 (t, J = 7.7
52
53
54
55
56
57
58
59
60

1
2
3
4 Hz, 1H, H₁₀), 7.29 (d, *J* = 3.7 Hz, 1H, H₃), 7.19 (d, *J* = 7.7 Hz, 1H, H₉), 7.09 (d, *J* = 3.7
5
6
7 Hz, 1H, H₄), 2.35 (s, 3H, CH₃). ¹³C NMR (75 MHz, DMSO-*d*₆) δ (ppm): 159.71, 156.85,
8
9
10 144.50, 138.82, 130.08, 129.59, 129.38, 125.23, 122.09, 120.29, 108.24, 21.35. FT-IR
11
12
13 (KBr) ν cm⁻¹: 3435, 2918, 2666, 2611, 2573, 1674, 1609, 1593, 1573, 1518, 1472, 1421,
14
15
16
17 1366, 1312, 1275, 1218, 1164, 1024, 788, 760. HRMS (ESI-QOrbitrap) *m/z*. calcd for
18
19
20
21 C₁₂H₁₀O₃ [M+H]⁺, 203.0703. Found 203.0702.
22
23

24 **5-(3-Aminophenyl)furan-2-carboxylic acid (5)**. Procedure A1. Starting compound:
25
26
27 methyl 5-(3-aminophenyl)furan-2-carboxylate (40 mg, 0.18 mmol, **22**). Yellow solid.
28
29
30
31 Yield: 33 mg, 0.16 mmol, 89%. Mp: 225 °C (dec.). TLC (DCM–MeOH 7:3): R_f = 0.33. ¹H-
32
33
34 NMR (300 MHz, DMSO-*d*₆) δ (ppm): 7.25 (d, *J* = 3.7 Hz, 1H, H₃), 7.10 (t, *J* = 7.9 Hz, 1H,
35
36
37 H₁₀), 6.99 (t, *J* = 2.0 Hz, 1H, H₇), 6.92 (m, 1H, H₁₁), 6.91 (d, *J* = 3.7 Hz, 1H, H₄), 6.56
38
39
40
41 (ddd, *J* = 7.9, 2.0, 1.0 Hz, 1H, H₉). ¹³C NMR (75 MHz, DMSO-*d*₆) δ (ppm): 159.79,
42
43
44
45 157.61, 149.65, 144.21, 130.12, 129.95, 120.11, 115.09, 112.75, 109.69, 107.49. FT-IR
46
47
48 (KBr) ν cm⁻¹: 3439, 3350, 3241, 3122, 3056, 2961, 2920, 2850, 1682, 1621, 1604, 1573,
49
50
51
52 1525, 1490, 1471, 1376, 1257, 959, 949, 803, 781. HRMS (ESI-QOrbitrap) *m/z*. calcd
53
54
55
56 C₁₁H₉NO₃ [M-H]⁻, 202.0510. Found 202.0512.
57
58
59
60

1
2
3
4 **5-(3-Carbamoylphenyl)furan-2-carboxylic acid (6)**. Procedure A1. Starting compound:
5
6
7 methyl 5-(3-carbamoylphenyl)furan-2-carboxylate (45 mg, 0.18 mmol, **15**). White solid.
8
9
10 Yield: 34 mg, 0.15 mmol, 81%. Mp: 250 °C. TLC (DCM–MeOH 7:3): R_f = 0.29. ^1H NMR
11
12 (300 MHz, $\text{DMSO-}d_6$) δ (ppm): 13.10-13.00 (bs exch. D_2O , 1H, COOH), 8.27 (s, 1H,
13
14 H_7), 8.11 (bs exch. D_2O , 1H, NH_2), 7.92 (d, J = 7.8 Hz, 1H, H_9), 7.86 (d, J = 7.8 Hz, 1H,
15
16 H_{11}), 7.55 (t, J = 7.8 Hz, 1H, H_{10}), 7.49 (bs exch. D_2O , 1H, NH_2), 7.33 (d, J = 3.6 Hz, 1H,
17
18 H_3), 7.19 (d, J = 3.6 Hz, 1H, H_4). ^{13}C NMR (75 MHz, $\text{DMSO-}d_6$) δ (ppm): 167.68,
19
20 159.69, 156.09, 144.93, 135.59, 129.69, 129.56, 128.19, 127.39, 123.90, 120.26,
21
22 108.92. FT-IR (KBr) ν cm^{-1} : 3451, 3188, 2920, 2649, 2527, 1682, 1598, 1518, 1449,
23
24 1403, 1299, 1273, 1160, 1025, 958, 942, 795, 761. HRMS (ESI-QOrbitrap) m/z . calcd
25
26 for $\text{C}_{12}\text{H}_{10}\text{NO}_4$ $[\text{M}+\text{H}]^+$, 232.0604. Found 232.0614.
27
28
29
30
31
32
33
34
35
36
37
38
39
40
41

42 **5-(3-(Methylcarbamoyl)phenyl)furan-2-carboxylic acid (7)**. Procedure A2. Starting
43
44 compound: methyl 5-(3-(methylcarbamoyl)phenyl)furan-2-carboxylate (41 mg, 0.17
45
46 mmol, **19**). Yellow solid. Yield: 87%. Mp: 159 °C. TLC (DCM–MeOH 7:3): R_f = 0.32. ^1H
47
48 NMR (300 MHz, $\text{DMSO-}d_6$) δ (ppm): 8.58 (q exch. D_2O , J = 4.5 Hz, 1H, NH), 8.22 (t, J =
49
50 1.7 Hz, 1H, H_7), 7.92 (dt, J = 7.8, 1.7 Hz, 1H, H_9), 7.82 (dt, J = 7.8, 1.7 Hz, 1H, H_{11}),
51
52
53
54
55
56
57
58
59
60

1
2
3
4 7.55 (t, $J = 7.8$ Hz, 1H, H₁₀), 7.33 (d, $J = 3.6$ Hz, 1H, H₃), 7.18 (d, $J = 3.6$ Hz, 1H, H₄),
5
6
7 2.80 (d, $J = 4.5$ Hz, 3H, CH₃). ¹³C NMR (75 MHz, DMSO-*d*₆) δ (ppm): 166.54, 159.67,
8
9
10 156.10, 144.87, 135.85, 129.70, 129.62, 127.83, 127.28, 123.42, 120.31, 108.95, 26.73.
11
12
13
14 FT-IR (KBr) ν cm⁻¹: 3324, 3116, 3066, 2925, 1718, 1692, 1649, 1584, 1549, 1521,
15
16
17 1481, 1468, 1423, 1407, 1310, 1260, 1220, 1158, 1026, 803, 760. HRMS (ESI-
18
19
20
21 QOrbitrap) m/z : calcd for C₁₃H₁₁NO₄ [M+H]⁺, 246.0761. Found 246.0761.
22
23

24 **5-(3-Sulfamoylphenyl)furan-2-carboxylic acid (8)**. Procedure A1. Starting compound:
25
26
27 methyl 5-(3-sulfamoylphenyl)furan-2-carboxylate (50 mg, 0.18 mmol, **20**). Yellow solid.
28
29
30
31 Yield: 40 mg, 0.15 mmol, 84%. Mp: 261 °C (dec.). TLC (DCM–MeOH 7:3): R_f = 0.24. ¹H
32
33
34 NMR (300 MHz, DMSO-*d*₆) δ (ppm): 13.22 (bs exch. D₂O, 1H, COOH), 8.21 (t, $J = 1.8$
35
36
37 Hz, 1H, H₇), 8.03 (dt, $J = 7.9, 1.8$ Hz, 1H, H₁₁), 7.81 (dt, $J = 7.9, 1.8$ Hz, 1H, H₉), 7.67 (t,
38
39
40
41 $J = 7.9$ Hz, 1H, H₁₀), 7.48 (s exch. D₂O, 2H, NH₂), 7.35 (d, $J = 3.7$ Hz, 1H, H₃), 7.26 (d, J
42
43
44 = 3.7 Hz, 1H, H₄). ¹³C NMR (75 MHz, DMSO-*d*₆) δ (ppm): 170.43, 159.61, 155.14,
45
46
47
48 145.55, 145.25, 130.28, 130.23, 128.10, 126.17, 121.31, 120.28, 109.67. FT-IR (KBr) ν
49
50
51
52
53
54
55
56
57
58
59
60 cm⁻¹: 3340, 3252, 2919, 2844, 2671, 2573, 1669, 1692, 1518, 1458, 1424, 1341, 1322,

1
2
3
4 1266, 1220, 1161, 1028, 890, 793, 762. HRMS (ESI-QOrbitrap) m/z . calcd for $C_{12}H_8O_5$
5
6
7 $[M-H]^-$, 266.0129. Found 266.0129.
8
9

10 **5-(3-Carboxyphenyl)furan-2-carboxylic acid (9)**. Procedure A1. Starting compound:
11
12 methyl 5-(3-(methoxycarbonyl)phenyl)furan-2-carboxylate (60 mg, 0.23 mmol, **21**).
13
14 White solid. Yield: 50 mg, 0.20 mmol, 88%. Mp > 300 °C. TLC (DCM–MeOH 8:2): R_f =
15
16
17 0.26. 1H NMR (300 MHz, $DMSO-d_6$) δ (ppm): 13.20 (2H, bs exch. D_2O , 2H, COOH),
18
19
20
21 8.30 (s, 1H, H_7), 8.04 (d, J = 7.8, 1H, H_9), 7.92 (d, J = 7.8, 1H, H_{11}), 7.60 (t, J = 7.8 Hz,
22
23
24 1H, H_{10}), 7.32 (d, J = 3.6 Hz, 1H, H_3), 7.25 (d, J = 3.6 Hz, 1H, H_4). ^{13}C NMR (75 MHz,
25
26
27
28 $DMSO-d_6$) δ (ppm): 167.2, 159.7, 155.6, 145.0, 132.2, 129.9, 129.8, 129.1, 125.2,
29
30
31
32 120.2, 119.2. FT-IR (KBr) ν cm^{-1} : 3435, 2966, 2917, 2851, 2661, 2546, 1681, 1612,
33
34
35 1521, 1455, 1420, 1298, 1165, 1030, 804 761. HRMS (ESI-QOrbitrap) m/z . calcd for
36
37
38
39 $C_{12}H_8O_5$ $[M-H]^-$, 231.0299. Found 231.0301.
40
41
42
43
44

45 **5-(3-Cyanophenyl)furan-2-carboxylic acid (10)**. Procedure A2. Starting compound:
46
47 methyl 5-(3-cyanophenyl)furan-2-carboxylate (46 mg, 0.20 mmol, **16**). White solid.
48
49 Yield: 38 mg, 0.18 mmol, 87%. Mp: 260 °C (dec.). TLC (DCM–MeOH 8:2): R_f = 0.20. 1H
50
51
52 NMR (300 MHz, $DMSO-d_6$) δ (ppm): 13.30 (bs exch D_2O , 1H, COOH), 8.28 (s, 1H, H_7),
53
54
55
56
57
58
59
60

1
2
3
4 8.10 (d, $J = 7.8$ Hz, 1H, H₉); 7.80 (d, $J = 7.8$ Hz, 1H, H₁₁), 7.69 (t, $J = 7.8$ Hz, 1H, H₁₀),
5
6
7 7.34 (s, 2H, H_{3,4}). ¹³C NMR (75 MHz, DMSO-*d*₆) δ (ppm): 159.61, 154.33, 145.60,
8
9
10 132.55, 130.87, 130.75, 129.00, 128.36, 120.12, 118.77, 112.81, 110.22. FT-IR (KBr) ν
11
12
13 cm⁻¹: 3112, 2915, 2850, 2666, 2576, 2231, 1710, 1686, 1608, 1572, 1519, 1475, 1436,
14
15
16
17 1318, 1289, 1232, 1174, 1033, 997, 819, 801, 761, 582. HRMS (ESI-QOrbitrap) m/z .
18
19
20
21 calcd for C₁₂H₇NO₃ [M-H]⁻, 212.0353. Found 212.0351.
22
23

24 **5-(3-cyanophenyl)furan-2-carboxamide (11)**. HATU (178 mg, 0.47 mmol) and *N,N*-
25
26 diisopropylethylamine (0.32 mL, 1.9 mmol) were added to a solution of 5-(3-
27
28 cyanophenyl)furan-2-carboxylic acid (100 mg, 0.47 mmol, **10**) in DMF (2.50 mL), and
29
30
31 the resulting mixture was stirred for 30 min at room temperature. Then, NH₄Cl (75 mg,
32
33
34 1.4 mmol) was added, and the stirring was continued for 2 more hours. After
35
36
37 completion, the reaction was neutralized with 1 M HCl and partitioned between EtOAc
38
39
40 and H₂O. The organic layer was washed three times with cold H₂O, dried over
41
42
43 anhydrous Na₂SO₄ and concentrated *in vacuo*.²⁵ The crude product was purified by
44
45
46
47
48
49 crystallization from DCM/hexane to afford an off-white solid. Yield: 32 mg, 0.15 mmol,
50
51
52
53
54
55
56 32%. Mp: 202 °C. TLC (DCM–MeOH 95:5): R_f = 0.27. ¹H-NMR (300 MHz, DMSO-*d*₆) δ
57
58
59
60

1
2
3
4 (ppm): 8.45 (t, $J = 1.7$ Hz, 1H, H₇), 8.21 (d, $J = 7.8$ Hz, 1H, H₁₁), 8.08 (bs exch. D₂O, 1H,
5
6
7 *NH*), 7.80 (d, $J = 7.8$, 1H, H₉), 7.65 (t, $J = 7.8$ Hz, 1H, H₁₀), 7.52 (bs exch. D₂O, 1H, *NH*),
8
9
10
11 7.25 (d, $J = 3.6$ Hz, 1H, H₃), 7.15 (d, $J = 3.6$ Hz, 1H, H₄). ¹³C NMR (75 MHz, DMSO-*d*₆)
12
13
14 δ (ppm): 159.51, 152.57, 148.48, 132.29, 131.06, 130.62, 129.01, 128.15, 118.96,
15
16
17 116.18, 112.66, 109.92. FT-IR (KBr) ν cm⁻¹: 3474, 3167, 2962, 2923, 2852, 2225, 1697,
18
19
20
21 1614, 1535, 1518, 1470, 1425, 1395, 1261, 1099, 1037, 958, 903, 893, 798. HRMS
22
23
24 (ESI-QOrbitrap) *m/z*. calcd for C₁₂H₈N₂O₂ [M+H]⁺, 213.0659. Found 213.0659.
25
26
27

28 **Methyl 5-bromofuran-2-carboxylate (12)**. Procedure D. Starting compound 5-bromo-2-
29
30
31 furoic acid (500 mg, 2.6 mmol). White solid. Yield: 480 mg, 2.3 mmol, 89%. Mp: 64 °C.
32
33
34
35 TLC (cyclohexane–EtOAc 8:2): R_f = 0.59. ¹H-NMR (300 MHz, CDCl₃) δ (ppm): 7.12 (d, J
36
37
38 = 3.5 Hz, 1H, H₃), 6.45 (d, $J = 3.5$ Hz, 1H, H₄), 3.89 (s, 3H, CH₃).
39
40
41

42 **Methyl 5-(3-chlorophenyl)furan-2-carboxylate (13)**. Procedure B. Starting compounds:
43
44
45 methyl 5-bromofuran-2-carboxylate (400 mg, 2.0 mmol, **12**) and (3-chlorophenyl)boronic
46
47
48 acid (407 mg, 2.6 mmol). The crude was purified by flash column chromatography
49
50
51
52 (cyclohexane–EtOAc 8:2) to give the desired product as a white solid. Yield: 321 mg,
53
54
55
56 1.4 mmol, 68%. Mp: 76 °C. TLC (cyclohexane– EtOAc 8:2): R_f = 0.53. ¹H-NMR (300
57
58
59
60

1
2
3
4 MHz, CDCl₃) δ (ppm): 7.76 (s, 1H, H₇), 7.64 (d, J = 7.3 Hz, 1H, H₁₁), 7.40 – 7.13 (m, 3H,
5
6
7 H_{3,9,10}), 6.75 (d, J = 3.6 Hz, 1H, H₄), 3.92 (s, 3H, CH₃).
8
9

10 **Methyl 5-(3-hydroxyphenyl)furan-2-carboxylate (14).** Procedure B. Starting
11
12 compounds: methyl 5-bromofuran-2-carboxylate (400 mg, 2.0 mmol, **12**) and (3-
13
14 hydroxyphenyl)boronic acid (359 mg, 2.6 mmol). The crude was purified by flash
15
16
17 column chromatography (cyclohexane–EtOAc 8:2) to give the desired product as a
18
19
20 white solid. Yield: 135 mg, 0.62 mmol, 31%. Mp: 149 °C. TLC (cyclohexane–EtOAc 8:2):
21
22
23 R_f = 0.23. ¹H-NMR (300 MHz, CDCl₃) δ (ppm): 7.51 – 7.10 (m, 4H, H_{3,7,10,11}), 6.85 (d, J =
24
25 7.6 Hz, 1H, H₉), 6.72 (d, J = 3.6 Hz, 1H, H₄), 5.34 (bs exch. D₂O, 1H, OH), 3.92 (s, 3H,
26
27
28 CH₃).
29
30
31
32
33
34
35
36
37

38 **Methyl 5-(3-carbamoylphenyl)furan-2-carboxylate (15).** Procedure B. Starting
39
40 compounds: methyl 5-bromofuran-2-carboxylate (400 mg, 2.0 mmol, **12**) and (3-
41
42 carbamoylphenyl)boronic acid (429 mg, 2.6 mol). The crude was purified by flash
43
44
45 column chromatography (DCM–EtOAc 7:3) to give the desired product as a white solid.
46
47
48
49 Yield: 123 mg, 0.5 mmol, 25%. Mp: 192 °C. TLC (cyclohexane–EtOAc 4:6): R_f = 0.24.
50
51
52
53
54
55
56 ¹H-NMR (300 MHz, CDCl₃) δ (ppm): 8.22 (t, J = 1.4 Hz, 1H, H₇), 7.94 (dt, J = 7.8, 1.4
57
58
59
60

1
2
3 Hz, 1H, H₉), 7.79 (dt, $J = 7.8, 1.4$ Hz, 1H, H₁₀), 7.52 (t, $J = 7.8$ Hz, 1H, H₁₁), 7.26 (d
4
5
6 partially hidden by solvent peak, $J = 3.6$ Hz, 1H, H₃), 6.83 (d, $J = 3.6$ Hz, 1H, H₄), 6.20
7
8
9
10 (bs exch. D₂O, 1H, NH), 5.66 (bs exch. D₂O, 1H, NH), 3.93 (s, 3H, CH₃).

11
12
13
14 **Methyl 5-(3-cyanophenyl)furan-2-carboxylate (16)**. Procedure B. Starting compounds:
15
16
17 methyl 5-bromofuran-2-carboxylate (400 mg, 2.0 mmol, **12**) and (3-cyanophenyl)boronic
18
19
20 acid (382 mg, 2.6 mmol). The crude was purified by flash column chromatography
21
22
23 (cyclohexane–EtOAc 8:2) to give the desired product as a white solid. Yield: 345 mg,
24
25
26
27 1.5 mmol, 75%. Mp: 149 °C. TLC (cyclohexane–EtOAc 8:2): $R_f = 0.33$. ¹H-NMR (300
28
29
30 MHz, CDCl₃) δ (ppm): 8.06 (s, 1H, H₇), 8.00 (d, $J = 7.8$ Hz, 1H, H₁₁), 7.62 (d, $J = 7.8$ Hz,
31
32
33 1H, H₉), 7.54 (t, $J = 7.8$ Hz, 1H, H₁₀), 7.26 (d partially hidden by solvent peak, $J = 3.6$
34
35
36 Hz, 1H, H₃), 6.83 (d, $J = 3.6$ Hz, 1H, H₄), 3.94 (s, 3H, CH₃).

37
38
39
40
41
42 **(5-(Methoxycarbonyl)furan-2-yl)boronic acid (17)**. Isopropylmagnesium chloride (2 M
43
44
45 in THF, 2.4 mmol) was added to a solution of bis[2-(*N,N*-dimethylamino)ethyl] ether (62
46
47
48 mg, 2.4 mmol) in THF (10 mL) under N₂ atmosphere. The resulting mixture was stirred
49
50
51
52 for 20 min at 10–15 °C, before methyl 5-bromofuran-2-carboxylate (400 mg, 2.0 mmol,
53
54
55
56 **12**) was added; the stirring was continued at room temperature for 30 min. Then,
57
58
59
60

1
2
3 trimethyl borate (416 mg, 4.0 mmol) was added at 0 °C and the reaction mixture was
4
5
6
7 stirred for 10 min. After quenching with diluted 1 M HCl, the reaction was extracted with
8
9
10 EtOAc (3 x 4 mL) and the organic layers were washed with brine, dried over anhydrous
11
12
13 Na₂SO₄ and evaporated *in vacuo*. The resulting brown solid was purified *via*
14
15
16
17 crystallization from hexane and EtOAc, to afford the desired product as a beige solid.
18
19
20
21 Yield: 255 mg, 1.5 mmol, 75%. Mp: 128 °C (dec.). TLC (cyclohexane–EtOAc 8:2): R_f =
22
23
24 0.54. ¹H-NMR (300 MHz, CDCl₃) δ (ppm): 7.19 (d, *J* = 3.5 Hz, 1H, H₃), 7.08 (d, *J* = 3.5
25
26
27 Hz, 1H, H₄), 3.91 (s, 3H, CH₃).¹²

31 **Methyl 5-(*m*-tolyl)furan-2-carboxylate (18).** Procedure C. Starting compounds: (5-
32
33
34 (methoxycarbonyl)furan-2-yl)boronic acid (221 mg, 1.3 mmol, **17**) and 1-bromo-3-
35
36
37 methylbenzene (171 mg, 1.0 mol). The crude was purified by flash column
38
39
40
41 chromatography (cyclohexane–EtOAc 8:2) to give the desired product as a white solid.
42
43
44
45 Yield: 112 mg, 0.52 mmol, 52%. Mp: 76 °C. TLC (cyclohexane–EtOAc 8:2): R_f = 0.73.
46
47
48
49 ¹H-NMR (300 MHz, CDCl₃) δ (ppm): 7.62 (s, 1H, H₇), 7.57 (d, *J* = 7.7 Hz, 1H, H₁₁), 7.30
50
51
52 (t, *J* = 7.7 Hz, 1H, H₁₀), 7.24 (d, *J* = 3.6 Hz, 1H, H₃), 7.16 (d, *J* = 7.7 Hz, 1H, H₉), 6.72 (d,
53
54
55
56 *J* = 3.6 Hz, 1H, H₄), 3.92 (s, 3H, OCH₃), 2.40 (s, 3H, CH₃).

1
2
3
4 **Methyl 5-(3-(methylcarbamoyl)phenyl)furan-2-carboxylate (19).** Procedure C. Starting
5
6
7 compounds: (5-(methoxycarbonyl)furan-2-yl)boronic acid (221 mg, 1.3 mmol, **17**) and 3-
8
9
10 bromo-*N*-methylbenzamide (213 mg, 1.0 mmol, **24**). The crude was purified by flash
11
12
13 column chromatography (cyclohexane–EtOAc 5:5) to give the desired product as a
14
15
16
17 yellow solid. Yield: 83 mg, 0.32 mmol, 32%. Mp: 76 °C. TLC (cyclohexane–EtOAc 5:5):
18
19
20 $R_f = 0.15$. $^1\text{H-NMR}$ (300 MHz, CDCl_3) δ (ppm): 8.11 (s, 1H, H₇), 7.86 (d, $J = 7.8$ Hz, 1H,
21
22
23 H₁₁), 7.73 (d, $J = 7.8$ Hz, 1H, H₉), 7.45 (t, $J = 7.8$ Hz, 1H, H₁₀), 7.23 (d, $J = 3.6$ Hz, 1H,
24
25
26 H₃), 6.78 (d, $J = 3.6$ Hz, 1H, H₄), 6.45 (bs exch. D₂O, 1H, NH), 3.91 (s, 3H, OCH₃), 3.03
27
28
29
30
31 (d, $J = 4.6$ Hz, 3H, NHCH₃).

32
33
34 **Methyl 5-(3-sulfamoylphenyl)furan-2-carboxylate (20).** Procedure C. Starting
35
36
37 compounds: (5-(methoxycarbonyl)furan-2-yl)boronic acid (221 mg, 1.3 mmol, **17**) and 3-
38
39
40 bromobenzenesulfonamide (237 mg, 1.0 mmol). The crude was purified by flash column
41
42
43 chromatography (cyclohexane–EtOAc 8:2) to give the desired product as a white solid.
44
45
46
47
48 Yield: 217 mg, 0.77 mmol, 77%. Mp: 238 °C. TLC (cyclohexane–EtOAc 5:5): $R_f = 0.38$.
49
50
51
52 $^1\text{H-NMR}$ (300 MHz, Acetone- d_6) δ (ppm): 8.32 (t, $J = 1.8$ Hz, 1H, H₇), 8.06 (ddd, $J = 7.8$,
53
54
55 1.8, 1.1 Hz, 1H, H₉), 7.91 (ddd, $J = 7.8, 1.8, 1.1$ Hz, 1H, H₁₁), 7.69 (t, $J = 7.8$ Hz, 1H,
56
57
58
59
60

1
2
3
4 H₁₀), 7.36 (d, $J = 3.7$ Hz, 1H, H₃), 7.21 (d, $J = 3.7$ Hz, 1H, H₄), 6.73 (bs exch. D₂O, 2H,
5
6
7 SO₂NH₂), 3.90 (s, 3H, CH₃).
8
9

10 **Methyl 5-(3-(methoxycarbonyl)phenyl)furan-2-carboxylate (21)**. Procedure C. Starting
11
12 compounds: (5-(methoxycarbonyl)furan-2-yl)boronic acid (221 mg, 1.3 mmol, **17**) and
13
14 methyl 3-bromobenzoate (214 mg, 1.0 mmol). The crude was purified by flash column
15
16
17 methyl 3-bromobenzoate (214 mg, 1.0 mmol). The crude was purified by flash column
18
19
20 chromatography (cyclohexane–EtOAc 8:2) to give the desired product as a white solid.
21
22
23
24 Yield: 125 mg, 0.48 mmol, 48%. Mp: 115 °C. TLC (cyclohexane–EtOAc 8:2): R_f = 0.51.
25
26
27
28 ¹H-NMR (300 MHz, CDCl₃) δ (ppm): 8.42 (s, 1H, H₇), 8.04–7.98 (m, 2H, H_{9,11}), 7.52 (t, J
29
30 = 7.8 Hz, 1H, H₁₀), 7.28 (d partially hidden by solvent peak, $J = 3.6$ Hz, 1H, H₃), 6.84 (d,
31
32 $J = 3.6$ Hz, 1H, H₄), 3.96 (s, 3H, CH₃), 3.93 (s, 3H, CH₃).
33
34
35
36
37

38 **Methyl 5-(3-aminophenyl)furan-2-carboxylate (22)**. To a solution of methyl 5-(3-
39
40 nitrophenyl)furan-2-carboxylate (232 mg, 1.0 mmol, **23**) in EtOAc (4 mL), SnCl₂ (57 mg,
41
42 0.3 mmol) was added and the mixture was refluxed for 5 h. After quenching by addition
43
44
45 of a saturated solution of NaHCO₃ until pH 7–8, the precipitated tin salts were eliminated
46
47
48
49 by filtration, and the aqueous phase was extracted with EtOAc (3 x 4 mL). The organic
50
51
52
53 layer was dried over Na₂SO₄, filtered and evaporated under vacuum. The crude residue
54
55
56
57
58
59
60

1
2
3 was purified by flash column chromatography (cyclohexane–EtOAc 8:2) to provide the
4
5
6
7 desired compound as a white solid. Yield: 165 mg, 0.76 mmol, 76%. Mp: 215 °C (dec.).
8
9
10 TLC (cyclohexane–EtOAc 8:2): $R_f = 0.45$. $^1\text{H NMR}$ (300 MHz, $\text{DMSO-}d_6$) δ (ppm): 7.36
11
12
13 (d, $J = 3.7$ Hz, 1H, H_3), 7.09 (t, $J = 7.8$ Hz, 1H, H_{11}), 7.00 (t, $J = 2.0$ Hz, 1H, H_7), 6.97 (d,
14
15
16
17 $J = 3.7$ Hz, 1H, H_4), 6.94 (d, $J = 7.8$ Hz, 1H, H_9), 6.57 (dd, $J = 7.8, 2.0$ Hz, 1H, H_9), 5.31
18
19
20
21 (bs exch. D_2O , 2H, NH_2), 3.81 (s, 3H, CH_3).²⁶
22
23

24 **Methyl 5-(3-nitrophenyl)furan-2-carboxylate (23)**. Procedure D. Starting compound: 5-
25
26
27 (3-nitrophenyl)furan-2-carboxylic acid (233 mg, 1.0 mmol). Light yellow solid. Yield: 215
28
29
30
31 mg, 0.87 mmol, 87%. Mp= 143 °C. TLC (cyclohexane–EtOAc 8:2) $R_f = 0.28$. $^1\text{H NMR}$
32
33
34 (300 MHz, CDCl_3) δ (ppm): 8.59 (t, $J = 2.0$ Hz, 1H, H_7), 8.20 (ddd, $J = 8.0, 2.0, 1.0$ Hz,
35
36
37
38 1H, H_{11}), 8.11 (ddd, $J = 8.0, 2.0, 1.0$ Hz, 1H, H_9), 7.62 (t, $J = 8.0$ Hz, 1H, H_{10}), 7.29 (d, J
39
40
41 = 3.6 Hz, 1H, H_3), 6.91 (d, $J = 3.6$ Hz, 1H, H_4), 3.95 (s, 3H, CH_3).
42
43
44

45 **3-Bromo-*N*-methylbenzamide (24)**. To a solution of 3-bromobenzoic acid (200 mg, 1.0
46
47
48 mmol) in THF (4 mL), HATU (570 mg, 1.5 mmol) and *N,N*-diisopropylethylamine (259
49
50
51 mg, 2.0 mmol) were added at 0 °C. The reaction mixture was stirred for 30 min at room
52
53
54
55 temperature. Methylamine (2 M in THF, 2.0 mmol) was added and the reaction was
56
57
58
59
60

1
2
3 stirred for 18 h. After completion, the mixture was extracted with EtOAc (3 x 4 mL). The
4
5
6 organic phase was dried over Na₂SO₄, filtered and concentrated under reduced
7
8
9 pressure. The resulting residue was purified by flash column chromatography (DCM–
10
11 MeOH 97:3) to afford a grey solid. Yield: 151 mg, 0.71 mmol, 71%. Mp: 91 °C. TLC
12
13 (DCM–MeOH 97:3): R_f = 0.33. ¹H-NMR (300 MHz, CDCl₃) δ (ppm): 7.89 (s, 1H, H₂),
14
15
16
17 7.66 (d, *J* = 7.8 Hz, 1H, H₆), 7.56 (d, *J* = 7.8 Hz, 1H, H₄), 7.23 (t, *J* = 7.8 Hz, 1H, H₅),
18
19
20
21 6.80 (bs exch. D₂O, 1H, NH), 2.95 (d, *J* = 4.7 Hz, 3H, CH₃).²⁷
22
23
24
25
26
27
28

29 *Production and purification of MbtI for crystallization trials*

30
31
32 *Escherichia coli* BL21 cells were transformed with a pET-28a plasmid (GenScript,
33
34 Piscataway, NJ, USA), bearing a codon-optimized open reading frame for MbtI. Two
35
36 transformed colonies were added to a starter medium (9.2 mL 2YT medium pH 7.0, 200
37
38 μL of 40% glucose, 100 μL of 1 M MgSO₄, 500 μL of 20X NPS buffer, 20 μL of 50
39
40 mg/mL kanamycin) and stirred at 37 °C and 180 rpm for 7 h. Then, sterile 5 L
41
42 Erlenmeyer flasks were filled with 1 L of 2YT medium pH 7.0, 50 mL of auto-induction
43
44 supplement (0.5% glycerol, 0.05% glucose, 0.2% α-lactose, 25 mM (NH₄)₂SO₄, 50 mM
45
46
47
48
49
50
51
52
53
54
55
56
57
58
59
60

1
2
3
4 KH₂PO₄, 50 mM Na₂HPO₄, 1 mM MgSO₄) and 2 mL of 50 mg/mL kanamycin; 1 mL of
5
6
7 the starter suspension was added to each flask and the culture was stirred at 180 rpm
8
9
10 for 4 h at 37 °C, and 12 h at 25 °C.
11
12

13
14 After centrifugation, the cell pellet was re-suspended using 50 mL of IMAC A solution
15
16
17 (25 mM Tris•HCl pH 8.5, 300 mM NaCl, 25 mM imidazole), with the addition of 50 µL of
18
19
20 Benzonase[®] Nuclease (Sigma-Aldrich) and a tablet of EDTA-free protease inhibitor
21
22
23 complex (cOmplete[™], Sigma-Aldrich). Then, the cells were lysed with a CF2 cell
24
25
26 disruptor (Constant Systems Ltd., Daventry, UK) and centrifuged. The supernatant was
27
28
29 charged on a 1 mL HisTrap[™] High Performance column (GE Healthcare, Chicago, IL,
30
31
32 USA) and eluted with a gradient obtained by mixing IMAC A and IMAC B (25 mM
33
34
35 Tris•HCl pH 8.5, 300 mM NaCl, 400 mM imidazole) solutions. Then, TEV protease (200
36
37
38 µL of a 10 mg/mL solution) was added to the protein solution to cleave the His-tag,
39
40
41
42 along with 5 µL of 1 M DTT (final concentration ≈ 100 mM). The resulting mixture was
43
44
45
46 dialyzed overnight at 4 °C in a solution containing 25 mM Hepes•NaOH pH 8.0, 150 mM
47
48
49 NaCl, 0.5 mM DTT. Subsequently, 40 mM imidazole was added to the dialyzed protein,
50
51
52
53 and the solution was loaded on a BioRad column charged with Ni-NTA resin, to remove
54
55
56
57
58
59
60

1
2
3 the His-tag. The column was washed with IMAC B, and the protein was concentrated to
4
5
6 about 1 mL, using 20 mL Vivaspin™ 15R Centrifugal Concentrators equipped with a
7
8
9
10 10000 Da cut-off filter (Sartorius, Göttingen, Germany). The supernatant was loaded on
11
12
13 a HiLoad 16/600 Superdex 200 exclusion chromatography column (GE Healthcare),
14
15
16 previously equilibrated with the eluent solution (25 mM Hepes·NaOH pH 8.0, 150 mM
17
18
19 NaCl, 1% glycerol). The fractions containing the protein were collected and
20
21
22 concentrated to allow the obtainment of the final purified protein solution at about 20
23
24
25
26
27 mg/mL concentration (calculated with a NanoDrop™ 1000, ThermoFisher Scientific);
28
29
30
31 the samples were flash-frozen with liquid nitrogen and stored at -80 °C.
32
33
34
35

36 *Crystallization of MbtI-10, MbtI-Mg²⁺ and MbtI-Ba²⁺ complexes*

37
38
39

40 The crystallization experiments were performed at 4 °C by the sitting drop vapor
41
42
43 diffusion technique in 96-well plates, according to established protocols at the
44
45
46 Crystallography Core Facility of the Institut Pasteur.²⁸ The trials were set up with a
47
48
49 Mosquito® crystal Nanoliter Protein Crystallization Robot (TTP Labtech, Melbourne,
50
51
52 UK); the plates were stored in a Rock Imager® 1000 (Formulatrix, Bedford, MA, USA)
53
54
55
56
57
58
59
60

1
2
3 and visually checked through the dedicated image repository, following a specific
4
5
6
7 timetable. The drops were obtained by mixing an equal amount of protein and reservoir
8
9
10 solutions to a final volume of 400 nL; the reservoir contained 150 μ L of the precipitant
11
12
13
14 mixture.
15

16
17 A solution of freshly purified MbtI was concentrated to 20 mg/mL in the gel filtration
18
19
20 buffer (25 mM Hepes·NaOH pH 8.0, 150 mM NaCl, 1% glycerol); the sodium salt of **10**,
21
22
23
24 dissolved in H₂O, was added to the protein to a final concentration of 5 mM and
25
26
27
28 incubated at 4 °C overnight. Prism-shaped crystals of up to 320 × 160 × 30 μ m grew
29
30
31 within two weeks in the presence of 20% PEG 3350 and 0.2 M solutions of different
32
33
34
35 sodium salts, among which sodium tartrate provided the best results. The previously
36
37
38 described protocol was also applied for the obtainment of the MbtI-Mg²⁺ and MbtI-Ba²⁺
39
40
41
42 crystals. MbtI-Mg²⁺ crystals (tabular, maximum side length: 160 μ m) grew within two
43
44
45 weeks in the presence of 1.75 M MgSO₄ and 0.1 M MES pH 6.5, while MbtI-Ba²⁺
46
47
48
49 crystals (prism, maximum side length: 270 μ m) grew within three weeks in the presence
50
51
52 of 5 mM chorismic acid barium salt, 0.04 M KH₂PO₄, 16% PEG 8000 and 16% glycerol.
53
54
55
56 The crystals were harvested with CryoLoops (Hampton Research, Aliso Viejo, CA,
57
58
59
60

1
2
3 USA), cryoprotected in a 1:1 mixture of paraffin and parathon oil (Hampton Research)
4
5
6
7 and flash-frozen by rapid immersion in liquid nitrogen.
8
9

10 11 *Data collection and structure solution*

12
13
14
15 Diffraction data were acquired at the SOLEIL Synchrotron (Saint-Aubin, France) on
16
17
18 the beamlines PROXIMA-1 for MbtI-10 complex and PROXIMA-2A for MbtI-Mg²⁺ and
19
20
21 MbtI-Ba²⁺, from crystals maintained at 100 K. The data were processed, scaled, and
22
23
24
25 analyzed using XDSME and autoPROC.^{29,30} The structures were solved with the
26
27
28
29 Molecular Replacement (MR) method through the program PHASER,³¹ available in the
30
31
32
33 CCP4 suite,³² using as model the PDB-deposited structure 3RV7.²⁰ The geometrical
34
35
36 restraints for the inhibitor **10** were generated with the Grade server
37
38
39 (<http://grade.globalphasing.org>), while restraints for the salicylate were obtained from
40
41
42
43 AceDRG.³³ All rebuilding and adjustments of the models were performed with COOT.³⁴
44
45
46
47 The refinement was carried out with BUSTER,³⁵ applying local structure similarity
48
49
50 restraints for non-crystallography symmetry (NCS) and a Translation-Libration-Screw
51
52
53
54 (TLS) model. The final validation was performed with MOLPROBITY and PHENIX.^{36,37}
55
56
57
58
59
60

Data collection, refinement, and model statistics are summarized in Table 2. Graphical representations were rendered with Pymol.³⁸

Table 2. Data collection, refinement, and model statistics of MbtI-10, MbtI-Mg²⁺ and MbtI-Ba²⁺.

	MbtI-10	MbtI-Mg ²⁺	MbtI-Ba ²⁺
Space group	P2 ₁	I422	P2 ₁
Unit-cell parameters			
<i>a</i> , <i>b</i> , <i>c</i> (Å)	88.336, 111.687, 94.998	193.97, 193.97, 257.03	88.04, 116.90 94.09
<i>α</i> , <i>β</i> , <i>γ</i> (°)	90, 92.67, 90	90, 90, 90	90, 91.60, 90
Resolution range (Å)	111.69 – 2.09 (2.13 – 2.09)	154.83 – 2.11 (2.15 – 2.11)	43.63 – 1.80 (1.85 – 1.80)
Wavelength (Å)	0.97856	0.98012	0.98012
No. unique reflections	108510 (5396)	131041 (6551)	173404 (11664)
Multiplicity	7.0 (7.1)	27.0 (26.5)	6.8 (6.5)
Completeness (%)	99.9 (99.9)	93.9 (85.6)	99.2 (90.3)
Average <i>I</i> /σ(<i>I</i>)	8.0 (2.1)	17.7 (1.4)	14.6 (1.0)

$R_{\text{pim}}^{\text{a}}$	0.063 (0.356)	0.028 (0.546)	0.030 (0.595)
CC(1/2)	0.990 (0.803)	0.998 (0.534)	0.999 (0.622)
<u>Refinement statistics</u>			
$R_{\text{work}}^{\text{b}}$	0.208	0.195	0.196
$R_{\text{free}}^{\text{b}}$	0.240	0.217	0.214
No. of non-H atoms ^c			
Protein	12651	13151	13228
Ligands	65	198	51
Water	878	797	1351
Average <i>B</i> -factors ^c			
Protein	43.33	51.97	35.98
Ligands	56.33	89.33	43.89
Water	44.14	53.14	42.82
Rms deviations ^c			
Bonds (Å)	0.012	0.012	0.012
Angles (°)	1.45	1.50	1.45
Molprobit Clashscore ^c			
	3.13	2.90	1.51
Ramachandran outliers ^c (%)			
	0.00	0.00	0.00
Ramachandran favoured ^c (%)			
	98.98	98.34	98.80
Rotamer outliers ^c (%)			
	1.09	1.11	1.11

C-beta outliers ^c (%)	0.00	0.00	0.00
PDB code	6ZA4	6ZA5	6ZA6

Data were indexed and scaled with XDSME (MbtI-Ba²⁺) or autoPROC (MbtI-10 and MbtI-Mg²⁺), applying, in the latter case, an anisotropic resolution cut-off *via* STARANISO as implemented in autoPROC.³⁰ $aR_{pim} = \sum h [1/(n_h - 1)]^{1/2} \sum i |<I_h> I_{h,i}| / \sum h \sum i I_{h,i}$, where I_h is the intensity of the unique reflection h , whereas I_i is the intensity of each of its symmetry-equivalent reflections. CC(1/2) according to Karplus.³⁹ $bR_{work} = \sum ||F_o| - |F_c|| / \sum |F_o|$, where F_o and F_c are the observed and calculated structure factor amplitudes. Five percent of the reflections were reserved for the calculation of R_{free} . ^cCalculated with phenix.validate.³⁷

MbtI enzymatic assays

MbtI was produced in recombinant form and purified, as previously reported.¹² The enzyme activity was determined by a fluorimetric assay, performed in a final volume of 400 μ L at 37 °C, in 50 mM Hepes pH 7.5, 5 mM MgCl₂, 1-2 μ M MbtI. The reactions were started by the addition of chorismic acid and monitored using a Perkin-Elmer LS3 fluorimeter (Ex. λ = 305 nm, Em. λ = 420 nm). Initial inhibition assays were carried out in the presence of 100 μ M of each compound (stock solution 20 mM in DMSO) and chorismic acid at a final concentration of 50 μ M. For the most potent inhibitors, the IC₅₀ and K_i were determined. For IC₅₀ determinations, the enzyme activity was measured at

1
2
3 different compound concentrations, and values were calculated according to the

4
5
6
7 Equation 1, with Origin 8 software:

$$A_{[I]} = A_{[0]} \times \left(1 - \frac{[I]}{[I] + IC_{50}}\right) \quad (\text{Equation 1})$$

8
9
10
11
12
13
14 where $A_{[I]}$ is the activity of the enzyme at inhibitor concentration $[I]$ and $A_{[0]}$ is the
15
16
17 activity of the enzyme without inhibitor.

18
19
20
21 The K_i was determined at different substrate $[S]$ and compound concentrations, using
22
23
24 Equation 2:

$$v = \frac{V_{\max}[S]}{[S] + K_m \left(1 + \frac{[I]}{K_i}\right)} \quad (\text{Equation 2})$$

25
26
27
28
29
30
31
32 To verify that the compounds were not pan-assay interference compounds (PAINS),
33
34
35 the inhibition was tested in the presence of 0.1 mg/mL of bovine serum albumin (BSA),
36
37
38 or 0.01% (v/v) Triton X-100 to confirm that they did not act as aggregators, and with 100
39
40
41
42 mM of 1,4-dithio-DL-threitol (DTT), to exclude an inhibition due to reaction with
43
44
45
46 cysteines.⁴⁰
47
48
49
50
51
52
53
54
55
56
57
58
59
60

Minimal inhibitory concentration determinations and siderophore production assay

The minimal inhibitory concentration MIC⁹⁹ of active compounds against *M. tuberculosis* H37Rv, was determined on Middlebrook 7H11 agar solid medium, as previously reported.¹¹ Additionally, MIC⁹⁹ against *M. bovis* BCG was determined in low-iron Chelated Sauton's medium, by the resazurin reduction assay method (REMA).^{41,42}

The siderophore activity was measured by the Universal CAS liquid assay.¹⁶ *M. bovis* cells were grown in 7H9 medium, subcultured in chelated Sauton's medium, and finally diluted to an OD₆₀₀ of 0.01 in chelated Sauton's containing different concentrations of compounds, in 96-well plates. After 15 days of incubation at 37 °C, cells were harvested. Supernatants were used to perform the CAS assay, while cell pellets were used for the determination of mycobactins. For the CAS assay, 100 µL of supernatant were mixed with 100 µL of CAS assay liquid solution in a 96-well plate, incubated 10 min at room temperature, and absorbance was read at 630 nm. The siderophore units were calculated using Equation 3:

$$\frac{A_r - A_s}{A_r} \times 100 \quad (\text{Equation 3})$$

1
2
3 where A_r is the absorbance at 630 nm of the blank medium with CAS assay solution
4
5
6
7 and A_s is the absorbance of the culture supernatants with CAS assay solution.
8
9

10 For mycobactin determination, cell pellets were extracted in EtOH overnight, then 0.1
11
12
13 M FeCl_3 in EtOH was added until no color change was observed. The mixture was
14
15
16
17 incubated at room temperature for 1 h. Mycobactins were extracted in CHCl_3 , washed
18
19
20
21 with H_2O and evaporated; then, the residue was dissolved in MeOH. The concentration
22
23
24 of mycobactins was determined by measuring the absorbance at 450 nm (1% solution
25
26
27 of mycobactins gives an absorbance of 42.8).
28
29
30
31

32 *Salicylic acid determination in MbtI purified protein*

33
34
35
36 To confirm the presence of salicylic acid in complex with the purified MbtI, the protein
37
38
39 was concentrated to 25 mg/mL and denatured by incubation at 95 °C for 10 min, to
40
41
42 liberate any bound ligand. After 15 min of centrifugation at 12000 rpm, the supernatant
43
44
45
46 was recovered and analyzed in UHPLC/MS. The chromatographic analysis was
47
48
49 performed with a UHPLC apparatus JASCO X-LC system (Easton, MD, USA), coupled
50
51
52
53 with a MS spectrometer Thermo Fisher Scientific LTQ XL ESI-MS/MS system.
54
55
56
57
58
59
60

1
2
3
4 Chromatography was performed on an Acquity column (Waters Corporation, Milford,
5
6
7 MA, USA), 3 μm particle size, 0.3 mL/min, gradient 10 min from 90:10 H₂O/MeCN to
8
9
10 100% MeCN, then 4 min in 100% MeCN. Run were also recorded at 220 nm. The
11
12
13 analyses were performed in full-scan from 120 and 2000 a.m.u., negative mode with [M-
14
15
16 H]⁻ at 137.11 a.m.u., and base peaks were analyzed with dependent scan method with
17
18
19 CID = 30 eV in order to confirm the structure. As a positive control, a solution of salicylic
20
21
22 acid (1 mg/mL, Sigma-Aldrich) was used, while the completely unrelated protein
23
24
25
26
27 pantothenate kinase, expressed in the same *E. coli* strain and purified using a similar
28
29
30
31 protocol to that of MbtI, was employed as negative control.
32
33
34
35

36 *Docking studies*

37
38
39
40 Compounds **10** and **11** were docked into the minimized average structure of MbtI,
41
42
43 complexed with the lead **I** in the absence of the Mg²⁺ ion.¹¹ The software Gold with
44
45
46 ChemScore fitness function was used.⁴³ The docking site was defined as the region
47
48
49 comprising all residues that stayed within 10 Å from the reference compound **I**. The best
50
51
52
53
54 docking poses were taken into consideration and subjected to MD simulations.
55
56
57
58
59
60

MD simulations

All simulations were performed using AMBER 16.⁴⁴ General amber force field (GAFF) parameters were assigned to the ligands, whereas partial charges were determined using the AM1-BCC method, as implemented in the Antechamber suite of AMBER 16. MD simulations were carried out employing the ff14SB force field at 300 K. The MbtI-10 complex was placed in a rectangular parallelepiped water-box and solvated with a 20 Å water cap by using the TIP3P explicit solvent model. Sodium ions were added as counterions in order to neutralize the system. Before MD simulations, two steps of minimization were performed; in the first stage, a position constraint of 500 kcal/(mol·Å²) was applied to keep the protein fixed, thus minimizing only water molecules. In the second stage, the whole system was energy-minimized through 5000 steps of steepest descent followed by conjugate gradient (CG), until a convergence of 0.05 kcal/(mol·Å²) and imposing a harmonic potential of 10 kcal/(mol·Å²) to the protein α carbon. Particle mesh Ewald (PME) electrostatics and periodic boundary conditions were used in the simulations. The time step of the simulations was 2 fs with a cutoff of 10 Å for the non-bonded interactions, while SHAKE algorithm was applied to keep all bonds involving

1
2
3 hydrogen atoms fixed. Constant-volume periodic boundary MD simulation was carried
4
5
6
7 out for the first 0.5 ns, during which the temperature of the system was raised from 0 to
8
9
10 300 K. Then, 110 ns of constant-pressure periodic boundary MD was performed at 300
11
12
13 K, using the Langevin thermostat in order to maintain constant the temperature of the
14
15
16 system. A harmonic force constraint of 10 kcal/(mol·Å²) was applied to the protein α
17
18
19 carbons during the first 10 ns, whereas in the last 100 ns no restraints were applied to
20
21
22 the system. All the obtained MD trajectories were analyzed using the Cpptraj program
23
24
25
26
27 implemented in AMBER 16.⁴⁴
28
29
30
31

32 ASSOCIATED CONTENT

33 34 35 36 Supporting Information

37
38
39 The Supporting Information (SI) contains additional synthetic schemes related to the
40
41
42 synthesis of compounds **5** and **11**; ¹H NMR, ¹³C NMR, FT-IR, HRMS spectra of final
43
44
45 compounds (**2-11**); ¹H NMR spectra of intermediates (**12-24**); crystallographic and
46
47
48 computational supplementary figures; molecular formula strings (SMILES) of final
49
50
51
52
53
54
55
56
57
58
59
60 compounds.

1
2
3 SI is available free of charge on the ACS Publications website at DOI:
4
5
6
7

8 **Accession codes**

9

10
11 PDB codes for the crystal structures of MbtI with 10, Mg²⁺ and Ba²⁺ are 6ZA4, 6ZA5
12
13 and 6ZA6, respectively. Authors will release the atomic coordinates upon article
14
15
16
17
18
19 publication.
20
21
22

23 **AUTHOR INFORMATION**

24 **Corresponding Authors**

25
26
27

28 *Marco Bellinzoni: marco.bellinzoni@pasteur.fr
29
30

31 *Stefania Villa: stefania.villa@unimi.it
32
33
34

35 **Author Contributions**

36
37
38

39 §These authors contributed equally.
40
41
42

43
44
45 Conceptualization of the work: F.M., S.V., L.R.C., T.T.; synthesis: M.M., S.V. A.G;
46
47

48
49 biological data: L.R.C., G.S., J.C.S.; crystallographic analysis: M.B., M.M., F.M.;
50
51

52
53 analytical data: E.P., G.B., S.V., A.P.; modeling: T.T., G.P.; writing-original draft
54
55
56
57
58
59
60

1
2
3 preparation, review and editing: F.M., M.M., S.V., T.T and M.B.; supervision: F.M.; all
4
5
6
7 authors revised and approved the final manuscript.
8
9

10 11 12 **Funding Sources**

13
14
15 This work was funded by University of Milan (Linea B) and the Italian Ministry of
16
17
18
19 Education, University and Research (MIUR): Dipartimenti di Eccellenza Program (2018–
20
21
22 2022) - Dept. of Biology and Biotechnology "L. Spallanzani", University of Pavia. Partial
23
24
25
26 support was also provided by institutional grants from Institut Pasteur and CNRS.
27
28
29

30 31 **Notes**

32
33
34 No potential conflict of interest was reported by the authors.
35
36
37
38

39 40 **ACKNOWLEDGMENTS**

41
42
43 The authors would like to thank Prof. Luca Costantino and Prof. Daniela Barlocco for
44
45
46 the HRMS data and the helpful support, and Prof. Flavio Rizzolio for the cell viability
47
48
49 assay. We are grateful to Ahmed Haouz, Patrick Weber and Cédric Pissis (Institut
50
51
52 Pasteur) for carrying out robot-driven crystallization screenings. We also acknowledge
53
54
55
56
57
58
59
60

1
2
3 the synchrotron sources Soleil (Saint-Aubin, France) and ESRF (Grenoble, France) for
4
5
6
7 granting access to their facilities, and their staff for helpful assistance on the respective
8
9
10 beamlines.
11
12
13

14 ABBREVIATIONS

15
16
17 Mtb, *Mycobacterium tuberculosis*; MbtI, *Mycobacterium tuberculosis* salicylate
18
19
20 synthase; SAR, structure-activity relationships; HTS, high-throughput screening; PAIN,
21
22
23 pan-assay interference compound; BSA, bovine serum albumin; MRC-5, normal human
24
25
26 fetal lung fibroblast cell line; MST, menaquinone-siderophore-tryptophan; ASU,
27
28
29 asymmetric unit; DMF, *N,N*-dimethylformamide; HATU, 1-
30
31
32 [bis(dimethylamino)methylene]-1*H*-1,2,3-triazolo[4,5-*b*]pyridinium 3-oxide
33
34
35
36
37 hexafluorophosphate; THF, tetrahydrofuran; DCM, dichloromethane; PEG, polyethylene
38
39
40 glycol; MES, 2-(*N*-morpholino)ethanesulfonic acid; DMSO, dimethyl sulfoxide; DTT, 1,4-
41
42
43 dithio-DL-threitol; BCG, *bacillus* Calmette-Guerin; OD, optical density; CAS, chrome
44
45
46 azurol S; CID, collision-induced dissociation; TIP3P, transferable intermolecular
47
48
49 potential with 3 points; a.m.u., atomic mass unit; MeCN, acetonitrile; PME, particle
50
51
52
53
54
55
56
57
58
59
60

1
2
3 mesh Ewald; GAFF, general Amber force field; CG, conjugate gradient; MD, molecular
4
5
6
7 dynamics.
8
9
10
11
12
13
14

15 REFERENCES

- 16
17
18
19 (1) World Health Organization. *Global Tuberculosis Report 2019*, Geneva, 2019.
20
21
22
23 (2) Harrison, A. J.; Yu, M.; Gårdenborg, T.; Middleditch, M.; Ramsay, R. J.; Baker, E.
24
25
26
27 N.; Lott, J. S. The Structure of MbtI from *Mycobacterium tuberculosis*, the First
28
29
30 Enzyme in the Biosynthesis of the Siderophore Mycobactin, Reveals It to Be a
31
32
33 Salicylate Synthase. *J. Bacteriol.* **2006**, *188* (17), 6081–6091.
34
35
36
37 <https://doi.org/10.1128/JB.00338-06>.
38
39
40
41 (3) Chao, A.; Sieminski, P. J.; Owens, C. P.; Goulding, C. W. Iron Acquisition in
42
43
44
45 *Mycobacterium tuberculosis*. *Chem. Rev.* **2019**, *119* (2), 1193–1220.
46
47
48
49 <https://doi.org/10.1021/acs.chemrev.8b00285>.
50
51
52
53 (4) Meneghetti, F.; Villa, S.; Gelain, A.; Barlocco, D.; Chiarelli, L. R.; Pasca, M. R.;
54
55
56
57
58
59
60

1
2
3
4 Costantino, L. Iron Acquisition Pathways as Targets for Antitubercular Drugs.

5
6
7 *Curr. Med. Chem.* **2016**, *23* (35), 4009–4026.

8
9
10 <https://doi.org/10.2174/0929867323666160607223747>.

11
12
13
14
15 (5) Kozlowski, M. C.; Tom, N. J.; Seto, C. T.; Seffler, A. M.; Bartlett, P. A. Chorismate-

16
17
18 Utilizing Enzymes Isochorismate Synthase, Anthranilate Synthase, and *p*-

19
20
21 Aminobenzoate Synthase: Mechanistic Insight through Inhibitor Design. *J. Am.*

22
23
24
25 *Chem. Soc.* **1995**, *117*(8), 2128–2140. <https://doi.org/10.1021/ja00113a002>.

26
27
28
29
30 (6) Meneely, K. M.; Sundlov, J. A.; Gulick, A. M.; Moran, G. R.; Lamb, A. L. An Open

31
32
33 and Shut Case: The Interaction of Magnesium with MST Enzymes. *J. Am. Chem.*

34
35
36
37 *Soc.* **2016**, *138*(29), 9277–9293. <https://doi.org/10.1021/jacs.6b05134>.

38
39
40
41 (7) Manos-Turvey, A.; Bulloch, E. M. M.; Rutledge, P. J.; Baker, E. N.; Lott, J. S.;

42
43
44 Payne, R. J. Inhibition Studies of *Mycobacterium tuberculosis* Salicylate Synthase

45
46
47 (MbtI). *ChemMedChem* **2010**, *5* (7), 1067–1079.

48
49
50
51 <https://doi.org/10.1002/cmdc.201000137>.

- 1
2
3
4 (8) Liu, Z.; Liu, F.; Aldrich, C. C. Stereocontrolled Synthesis of a Potential Transition-
5
6
7 State Inhibitor of the Salicylate Synthase MbtI from *Mycobacterium tuberculosis*.
8
9
10 *J. Org. Chem.* **2015**, *80* (13), 6545–6552. <https://doi.org/10.1021/acs.joc.5b00455>.
11
12
13
14
15 (9) Vasan, M.; Neres, J.; Williams, J.; Wilson, D. J.; Teitelbaum, A. M.; Remmel, R.
16
17
18 P.; Aldrich, C. C. Inhibitors of the Salicylate Synthase (MbtI) from *Mycobacterium*
19
20
21 *tuberculosis* Discovered by High-Throughput Screening. *ChemMedChem* **2010**, *5*
22
23
24
25 (12), 2079–2087. <https://doi.org/10.1002/cmdc.201000275>.
26
27
28
29
30 (10) Zhang, X.-K.; Liu, F.; Fiers, W. D.; Sun, W.-M.; Guo, J.; Liu, Z.; Aldrich, C. C.
31
32
33 Synthesis of Transition-State Inhibitors of Chorismate Utilizing Enzymes from
34
35
36 Bromobenzene *Cis* -1,2-Dihydrodiol. *J. Org. Chem.* **2017**, *82* (7), 3432–3440.
37
38
39
40 <https://doi.org/10.1021/acs.joc.6b02801>.
41
42
43
44
45 (11) Chiarelli, L. R.; Mori, M.; Barlocco, D.; Beretta, G.; Gelain, A.; Pini, E.; Porcino,
46
47
48 M.; Mori, G.; Stelitano, G.; Costantino, L.; Lapillo, M.; Bonanni, D.; Poli, G.;
49
50
51
52 Tuccinardi, T.; Villa, S.; Meneghetti, F. Discovery and Development of Novel
53
54
55 Salicylate Synthase (MbtI) Furanic Inhibitors as Antitubercular Agents. *Eur. J.*
56
57
58
59
60

1
2
3
4 *Med. Chem.* **2018**, *155*, 754–763. <https://doi.org/10.1016/j.ejmech.2018.06.033>.
5
6
7

- 8 (12) Chiarelli, L. R.; Mori, M.; Beretta, G.; Gelain, A.; Pini, E.; Sammartino, J. C.;
9
10
11 Stelitano, G.; Barlocco, D.; Costantino, L.; Lapillo, M.; Poli, G.; Caligiuri, I.;
12
13
14 Rizzolio, F.; Bellinzoni, M.; Tuccinardi, T.; Villa, S.; Meneghetti, F. New Insight
15
16 into Structure-Activity of Furan-Based Salicylate Synthase (MbtI) Inhibitors as
17
18 Potential Antitubercular Agents. *J. Enzyme Inhib. Med. Chem.* **2019**, *34* (1), 823–
19
20
21
22 828. <https://doi.org/10.1080/14756366.2019.1589462>.
23
24
25
26
27
28
29

- 30 (13) McDonald, I. M.; Black, J. W.; Buck, I. M.; Dunstone, D. J.; Griffin, E. P.; Harper,
31
32
33 E. A.; Hull, R. A. D.; Kalindjian, S. B.; Lilley, E. J.; Linney, I. D.; Pether, M. J.;
34
35
36
37 Roberts, S. P.; Shaxted, M. E.; Spencer, J.; Steel, K. I. M.; Sykes, D. A.; Walker,
38
39
40 M. K.; Watt, G. F.; Wright, L.; Wright, P. T.; Xun, W. Optimization of 1,3,4-
41
42
43
44 Benzotriazepine-Based CCK₂ Antagonists to Obtain Potent, Orally Active
45
46
47 Inhibitors of Gastrin-Mediated Gastric Acid Secretion. *J. Med. Chem.* **2007**, *50*
48
49
50
51 (13), 3101–3112. <https://doi.org/10.1021/jm070139l>.
52
53
54

- 55 (14) Baell, J. B.; Holloway, G. A. New Substructure Filters for Removal of Pan Assay
56
57
58
59
60

- 1
2
3
4 Interference Compounds (PAINS) from Screening Libraries and for Their
5
6
7 Exclusion in Bioassays. *J. Med. Chem.* **2010**, *53* (7), 2719–2740.
8
9
10 <https://doi.org/10.1021/jm901137j>.
11
12
13
14
15 (15) Brosch, R.; Philipp, W. J.; Stavropoulos, E.; Colston, M. J.; Cole, S. T.; Gordon, S.
16
17
18 V. Genomic Analysis Reveals Variation between *Mycobacterium tuberculosis*
19
20
21 H37Rv and the Attenuated *M. tuberculosis* H37Ra Strain. *Infect. Immun.* **1999**, *67*
22
23
24
25 (11), 5768–5774. <https://doi.org/10.1128/iai.67.11.5768-5774.1999>.
26
27
28
29
30 (16) Schwyn, B.; Neilands, J. B. Universal Chemical Assay for the Detection and
31
32
33 Determination of Siderophores. *Anal. Biochem.* **1987**, *160* (1), 47–56.
34
35
36
37 [https://doi.org/10.1016/0003-2697\(87\)90612-9](https://doi.org/10.1016/0003-2697(87)90612-9).
38
39
40
41 (17) Ferrer, S.; Martí, S.; Andrés, J.; Moliner, V.; Tuñón, I.; Bertrán, J. Molecular
42
43
44 Mechanism of Chorismate Mutase Activity of Promiscuous MbtI. *Theor. Chem.*
45
46
47
48 *Acc.* **2011**, *128* (4–6), 601–607. <https://doi.org/10.1007/s00214-010-0773-z>.
49
50
51
52
53 (18) Ferrer, S.; Martí, S.; Moliner, V.; Tuñón, I.; Bertrán, J. Understanding the Different
54
55
56
57
58
59
60

- 1
2
3
4 Activities of Highly Promiscuous MbtI by Computational Methods. *Phys. Chem.*
5
6
7 *Chem. Phys.* **2012**, *14* (10), 3482. <https://doi.org/10.1039/c2cp23149b>.
8
9
10
11 (19) Ziebart, K. T.; Toney, M. D. Nucleophile Specificity in Anthranilate Synthase,
12
13
14 Aminodeoxychorismate Synthase, Isochorismate Synthase, and Salicylate
15
16
17
18 Synthase. *Biochemistry* **2010**, *49* (13), 2851–2859.
19
20
21
22 <https://doi.org/10.1021/bi100021x>.
23
24
25
26 (20) Chi, G.; Manos-Turvey, A.; O'Connor, P. D.; Johnston, J. M.; Evans, G. L.; Baker,
27
28
29 E. N.; Payne, R. J.; Lott, J. S.; Bulloch, E. M. M. Implications of Binding Mode and
30
31
32
33 Active Site Flexibility for Inhibitor Potency against the Salicylate Synthase from
34
35
36
37 *Mycobacterium tuberculosis*. *Biochemistry* **2012**, *51* (24), 4868–4879.
38
39
40
41 <https://doi.org/10.1021/bi3002067>.
42
43
44
45 (21) Dudev, T.; Cowan, J. A.; Lim, C. Competitive Binding in Magnesium Coordination
46
47
48
49 Chemistry: Water versus Ligands of Biological Interest. *J. Am. Chem. Soc.* **1999**,
50
51
52 *121* (33), 7665–7673. <https://doi.org/10.1021/JA984470T>.
53
54
55
56
57
58
59
60

- 1
2
3
4 (22) Zwahlen, J.; Kolappan, S.; Zhou, R.; Kisker, C.; Tonge, P. J. Structure and
5
6
7 Mechanism of MbtI, the Salicylate Synthase from *Mycobacterium tuberculosis*.
8
9
10 *Biochemistry* **2007**, *46* (4), 954–964. <https://doi.org/10.1021/bi060852x>.
11
12
13
14
15 (23) Kerbarh, O.; Chirgadze, D. Y.; Blundell, T. L.; Abell, C. Crystal Structures of
16
17
18 *Yersinia enterocolitica* Salicylate Synthase and Its Complex with the Reaction
19
20
21 Products Salicylate and Pyruvate. *J. Mol. Biol.* **2006**, *357* (2), 524–534.
22
23
24
25 <https://doi.org/10.1016/J.JMB.2005.12.078>.
26
27
28
29
30 (24) Pini, E.; Poli, G.; Tuccinardi, T.; Chiarelli, L.; Mori, M.; Gelain, A.; Costantino, L.;
31
32
33 Villa, S.; Meneghetti, F.; Barlocco, D. New Chromane-Based Derivatives as
34
35
36 Inhibitors of *Mycobacterium tuberculosis* Salicylate Synthase (MbtI): Preliminary
37
38
39 Biological Evaluation and Molecular Modeling Studies. *Molecules* **2018**, *23* (7),
40
41
42
43 1506. <https://doi.org/10.3390/molecules23071506>.
44
45
46
47
48 (25) Skerlj, R. T.; Bourque, E. M. J.; Lansbury, P. T.; Greenlee, W. J.; Good, A. C.
49
50
51 Imidazo [1,5-a]Pyrimidinyl Carboxamide Compounds and Their Use in the
52
53
54 Treatment of Medical Disorders. WO2017176961 (A1), 2017.
55
56
57
58
59
60

- 1
2
3
4 (26) Porta, F.; Gelain, A.; Barlocco, D.; Ferri, N.; Marchianò, S.; Cappello, V.; Basile,
5
6
7 L.; Guccione, S.; Meneghetti, F.; Villa, S. A Field-Based Disparity Analysis of New
8
9
10 1,2,5-Oxadiazole Derivatives Endowed with Antiproliferative Activity. *Chem. Biol.*
11
12
13 *Drug Des.* **2017**, *90*, 820–839. <https://doi.org/10.1111/cbdd.13003>.
14
15
16
17
18 (27) Kemp, M. I.; Woodrow, M. D. Cyanopyrrolidine Derivatives as Inhibitors for
19
20
21 DUBs. WO2017109488 (A1), 2017.
22
23
24
25
26 (28) Weber, P.; Pissis, C.; Navaza, R.; Mechaly, A. E.; Saul, F.; Alzari, P. M.; Haouz,
27
28
29 A. High-Throughput Crystallization Pipeline at the Crystallography Core Facility of
30
31
32 the Institut Pasteur. *Molecules* **2019**, *24* (24), 4451.
33
34
35
36
37 <https://doi.org/10.3390/molecules24244451>.
38
39
40
41 (29) Legrand, P. XDSME: XDS Made Easier. 2017.
42
43
44
45
46 (30) Vonrhein, C.; Flensburg, C.; Keller, P.; Sharff, A.; Smart, O.; Paciorek, W.;
47
48
49 Womack, T.; Bricogne, G. Data Processing and Analysis with the AutoPROC
50
51
52 Toolbox. *Acta Crystallogr. Sect. D Biol. Crystallogr.* **2011**, *67* (4), 293–302.
53
54
55
56
57
58
59
60

1
2
3
4 <https://doi.org/10.1107/S0907444911007773>.

- 5
6
7
8 (31) McCoy, A. J.; Grosse-Kunstleve, R. W.; Adams, P. D.; Winn, M. D.; Storoni, L. C.;
9
10
11 Read, R. J. *Phaser Crystallographic Software*. *J. Appl. Crystallogr.* **2007**, *40* (4),
12
13
14
15 658–674. <https://doi.org/10.1107/S0021889807021206>.

- 16
17
18
19 (32) Winn, M. D.; Ballard, C. C.; Cowtan, K. D.; Dodson, E. J.; Emsley, P.; Evans, P.
20
21
22
23 R.; Keegan, R. M.; Krissinel, E. B.; Leslie, A. G. W.; McCoy, A.; McNicholas, S. J.;
24
25
26
27 Murshudov, G. N.; Pannu, N. S.; Potterton, E. A.; Powell, H. R.; Read, R. J.;
28
29
30 Vagin, A.; Wilson, K. S. Overview of the *CCP4* Suite and Current Developments.
31
32
33
34 *Acta Crystallogr. Sect. D Biol. Crystallogr.* **2011**, *67* (4), 235–242.
35
36
37 <https://doi.org/10.1107/S0907444910045749>.

- 38
39
40
41 (33) Long, F.; Nicholls, R. A.; Emsley, P.; Gražulis, S.; Merkys, A.; Vaitkus, A.;
42
43
44
45 Murshudov, G. N. AceDRG: A Stereochemical Description Generator for Ligands.
46
47
48
49 *Acta Crystallogr. Sect. D Struct. Biol.* **2017**, *73* (2), 112–122.
50
51
52 <https://doi.org/10.1107/S2059798317000067>.

- 1
2
3
4 (34) Emsley, P.; Cowtan, K. *Coot*: Model-Building Tools for Molecular Graphics. *Acta*
5
6
7 *Crystallogr. Sect. D Biol. Crystallogr.* **2004**, *60* (12), 2126–2132.
8
9
10 <https://doi.org/10.1107/S0907444904019158>.
11
12
13
14
15 (35) Bricogne, G.; Blanc, E.; Brandl, M.; Flensburg, C.; Keller, P.; Paciorek, W.;
16
17
18 Roversi, P.; Sharff, A.; Smart, O. S.; Vonrhein, C.; Womack, T. O. BUSTER
19
20
21
22 Version 2.10.3. Global Phasing Ltd.: Cambridge, UK 2017.
23
24
25
26 (36) Chen, V. B.; Arendall, W. B.; Headd, J. J.; Keedy, D. A.; Immormino, R. M.;
27
28
29
30 Kapral, G. J.; Murray, L. W.; Richardson, J. S.; Richardson, D. C. *MolProbity*: All-
31
32
33
34 Atom Structure Validation for Macromolecular Crystallography. *Acta Crystallogr.*
35
36
37 *Sect. D Biol. Crystallogr.* **2010**, *66* (1), 12–21.
38
39
40 <https://doi.org/10.1107/S0907444909042073>.
41
42
43
44
45 (37) Adams, P. D.; Afonine, P. V.; Bunkóczi, G.; Chen, V. B.; Davis, I. W.; Echols, N.;
46
47
48
49 Headd, J. J.; Hung, L.-W.; Kapral, G. J.; Grosse-Kunstleve, R. W.; McCoy, A. J.;
50
51
52
53 Moriarty, N. W.; Oeffner, R.; Read, R. J.; Richardson, D. C.; Richardson, J. S.;
54
55
56
57 Terwilliger, T. C.; Zwart, P. H. *PHENIX*: A Comprehensive Python-Based System
58
59
60

1
2
3 for Macromolecular Structure Solution. *Acta Crystallogr. Sect. D Biol. Crystallogr.*

4
5
6
7 **2010**, *66* (2), 213–221. <https://doi.org/10.1107/S0907444909052925>.

8
9
10
11 (38) Schrödinger, L. *The PyMOL Molecular Graphics System, Version 1.8*, 2015.

12
13
14
15 (39) Karplus, P. A.; Diederichs, K. Linking Crystallographic Model and Data Quality.

16
17
18
19 *Science* **2012**, *336* (6084), 1030–1033. <https://doi.org/10.1126/science.1218231>.

20
21
22
23 (40) Dahlin, J. L.; Nissink, J. W. M.; Strasser, J. M.; Francis, S.; Higgins, L.; Zhou, H.;

24
25
26
27 Zhang, Z.; Walters, M. A. PAINS in the Assay: Chemical Mechanisms of Assay

28
29
30
31 Interference and Promiscuous Enzymatic Inhibition Observed during a Sulfhydryl-

32
33
34 Scavenging HTS. *J. Med. Chem.* **2015**, *58* (5), 2091–2113.

35
36
37
38 <https://doi.org/10.1021/jm5019093>.

39
40
41
42 (41) Siegrist, M. S.; Unnikrishnan, M.; McConnell, M. J.; Borowsky, M.; Cheng, T. Y.;

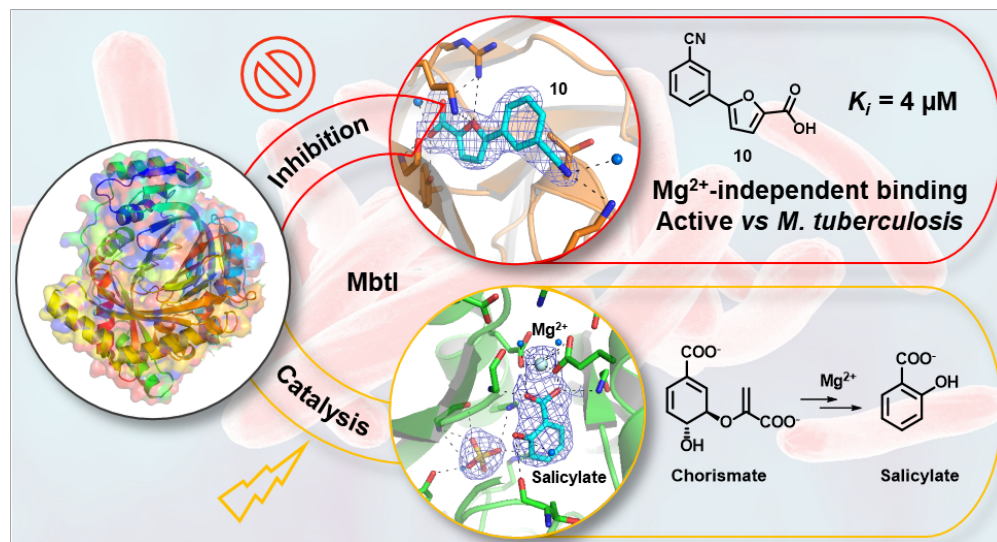
43
44
45
46 Siddiqi, N.; Fortune, S. M.; Moody, D. B.; Rubin, E. J. Mycobacterial Esx-3 Is

47
48
49
50 Required for Mycobactin-Mediated Iron Acquisition. *Proc. Natl. Acad. Sci. U. S. A.*

51
52
53
54 **2009**, *106* (44), 18792–18797. <https://doi.org/10.1073/pnas.0900589106>.

- 1
2
3
4 (42) Palomino, J. C.; Martin, A.; Camacho, M.; Guerra, H.; Swings, J.; Portaels, F.
5
6
7 Resazurin Microtiter Assay Plate: Simple and Inexpensive Method for Detection of
8
9
10 Drug Resistance in *Mycobacterium tuberculosis*. *Antimicrob. Agents Chemother.*
11
12
13
14 **2002**, *46* (8), 2720–2722. <https://doi.org/10.1128/AAC.46.8.2720-2722.2002>.
15
16
17
18 (43) Verdonk, M. L.; Cole, J. C.; Hartshorn, M. J.; Murray, C. W.; Taylor, R. D.
19
20
21
22 Improved Protein-Ligand Docking Using GOLD. *Proteins Struct. Funct. Genet.*
23
24
25 **2003**, *52* (4), 609–623. <https://doi.org/10.1002/prot.10465>.
26
27
28
29
30 (44) Case, D. A.; Berryman, J. T.; Betz, R. M.; Cerutti, D. S.; Cheatham III, T. E.;
31
32
33 Darden, T. A.; Duke, R. E.; Giese, T. J.; Gohlke, H.; Goetz, A. W.; Homeyer, N.;
34
35
36
37 Izadi, S.; Janowski, P.; Kaus, J.; Kovalenko, A.; Lee, T. S.; LeGrand, S.; Li, P.;
38
39
40
41 Luchko, T.; Luo, R.; Madej, B.; Merz, K. M.; Monard, G.; Needham, P.; Nguyen,
42
43
44 H.; Nguyen, H. T.; Omelyan, I.; Onufriev, A.; Roe, D. R.; Roitberg, A.; Salomon-
45
46
47 Ferrer, R.; Simmerling, C. L.; Smith, W.; Swails, J.; Walker, R. C.; Wang, J.; Wolf,
48
49
50
51 R. M.; Wu, X.; York, D. M.; Kollman, P. A. AMBER, Version 14. San Francisco,
52
53
54 CA 2015.
55
56
57
58
59
60

1
2
3
4
5
6
7
8
9
10
11
12
13
14
15
16
17
18
19
20
21
22
23
24
25
26
27
28
29
30
31
32
33
34
35
36
37
38
39
40
41
42
43
44
45
46
47
48
49
50
51
52
53
54
55
56
57
58
59
60



82x44mm (300 x 300 DPI)